UNIVERSITY OF THE WITWATERSRAND, JOHANNESBURG

SCHOOL OF MECHANICAL, INDUSTRIAL & AERONAUTICAL ENGINEERING

# Maximizing Solar Energy Harnessing For Sustainable Farming

**GROUP 2**


| Name | Student Number |
|---|---|
| Banda Willbes | 2109005 |
| Mbanzu Richelet Malembi | 2116615 |
| Philani Dlamini | 2135214 |
| Mokoena Tumiso | 2320283 |


A Mechatronics assignment report submitted to the Faculty of Engineering and the Built Environment, University of the Witwatersrand, Johannesburg, in partial fulfilment of the requirements for the degree of Bachelor of Science in Engineering.

Johannesburg, May 2024

# Executive Summary

This project aimed to design and implement a dual-axis solar tracker to optimize solar energy absorption for agricultural applications in Bredasdorp. The system combines azimuth and zenith rotations to provide full 3D orientation control, enabling the solar panels to follow the sun accurately throughout the day. The azimuth rotation handles horizontal movement, while the zenith rotation manages vertical adjustments, ensuring the panels capture maximum sunlight from sunrise to sunset.

Comprehensive analyses of the uncontrolled system's transient response and stability characteristics revealed partial stability, highlighting the need for a control system. A PID controller was implemented, demonstrating robust performance by maintaining system stability and minimizing tracking errors. The controlled system exhibited a steady-state error of 2.01%, a rise time of 0.264 seconds, and a settling time of 1.42 seconds, meeting all specified performance criteria. The dual-axis tracker improves solar panel efficiency by approximately 30% compared to single-axis trackers.

The success of this project underscores the importance of interdisciplinary collaboration, combining expertise from industrial, electrical, and information systems engineering to enhance the system's design and functionality. Despite challenges such as varying schedules and availability, the team's dedication and effective communication ensured the project's completion. Ultimately, the dual-axis solar tracker significantly boosts solar energy absorption, providing a reliable and sustainable power source for farming operations in Bredasdorp.

# Table Of Contents

# List Of Figures

# List Of Tables

# 1. INTRODUCTION

## 1.1 Project Background

In the captivating landscapes of the Western Cape's River deltas, where agriculture flourishes amidst the serenity of nature, resides the thriving farming town of Bredasdorp. Situated at sea level, this region basks in uninterrupted sunlight from the break of dawn to the gentle embrace of dusk.

Historically, farms in this region have relied primarily on conventional power sources to power irrigation pumps, which pull water from surrounding rivers for crop growth [1]. However, the reliance on non-renewable energy has substantial problems. Not only does it contribute to carbon emissions and environmental degradation, but it also exposes farmers to growing energy costs and inconsistent power supplies due to load shedding, particularly during high demand periods [2].

The decision to focus on Bredasdorp stems from an in-depth analysis of different factors critical to the development of an alternative clean energy source. At the outset, the town's strategic location at sea level provides an abundance of direct sunlight throughout the day, creating an ideal setting for solar energy harvesting. Additionally, the Western Cape's agricultural terrain, particularly in river deltas, provides a unique opportunity to easily integrate solar technology into existing irrigation systems [3].

*Figure 1: Centre Pivot Irrigation System [4]*

## 1.2 Project Objectives & Task Execution Methodology

For this project, a control system will be designed for efficient tracking of the sun's path, ensuring that the solar panel maintains the most optimal angle for energy absorption throughout the day for farming purposes in Bredasdorp. The harnessed solar energy will primarily be used to power pumps which draw water from the river to the centre pivot irrigation system, which is responsible for crop watering, as shown in figure 1.

To ensure precise direct sunlight tracking, online databases will be used to collect solar position data particular to Bredasdorp. This data will show the sun's position in the sky throughout the year. In addition, a nonlinear model will be developed to accurately represent the tracker system's dynamic behaviour. This model will be crucial in evaluating the uncontrolled system's performance in both the time domain (transient response) and the frequency domain (stability characteristics).

# 2. INFORMATION RESOURCES

## 2.1 Operating Environment Conditions

The environment has an inevitable effect on the evolution and design of control systems. Addressing these is critical for informed decision making and risk analysis imposed by the environment on the control system, this section discusses the effect of the environment in depth.

### 2.1.1 Sunlight Consistency

The notion of constant sunlight is not feasible given the sun's position, which changes throughout the day and seasons. Cloud cover, seasonal shifts, and atmospheric variables all contribute to variations in sun intensity as shown below [9].

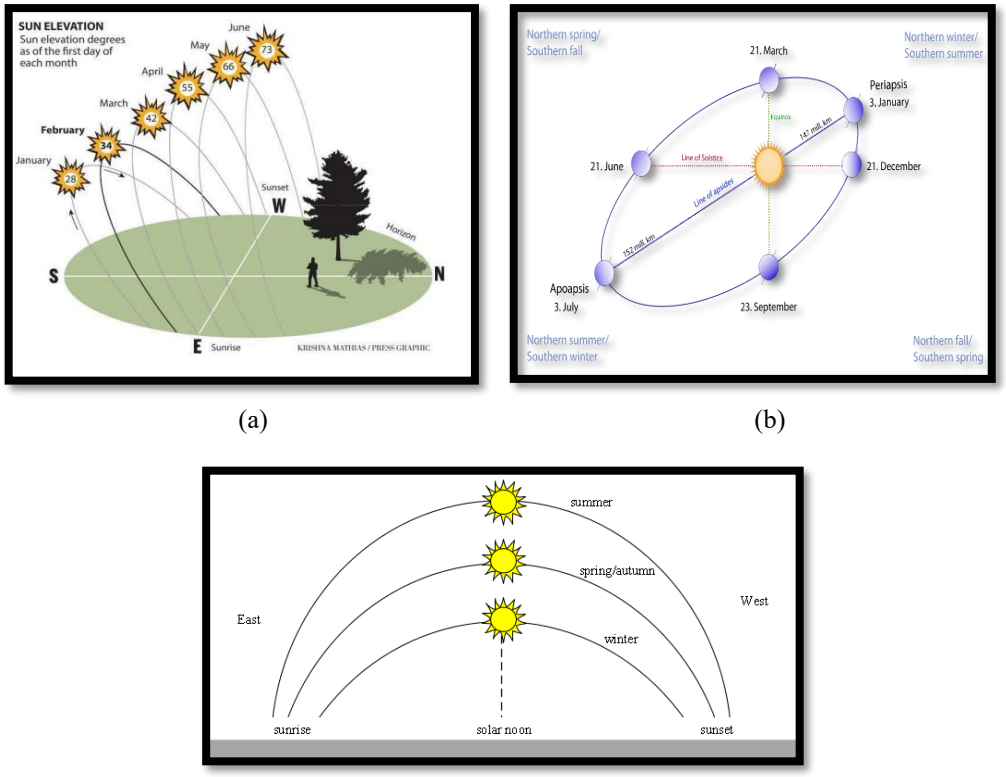


(a) (b)

(c)

*Figure 2: Trajectory Of The Sun Throughout The Year [8] [9] [10]*

These fluctuations need a more detailed understanding of solar radiation patterns, as well as the adoption of flexible technologies to maximize energy efficiency.

### 2.1.2 Factors Affecting Earth-Sun Energy [11]

- **Greenhouse Gases**
  - Increased amount of greenhouse gases affects the energy balance therefore acts as appositive feedback loop which increases warming.

- **Cloud Cover**
  - Clouds block the sun's incoming radiation therefore reducing the incoming solar energy thus reflecting back to space.

- **Atmospheric Aerosols**
  - Aerosols change the frequency of cloud size, occurrence and rainfall amounts, therefore an increase in aerosols will produce more clouds and high chances of rainfall.

- **Surface Absorption and reflection**
  - The surface reflects 30% of the sun's energy that was received

### 2.1.3 Uniform Terrain

Terrain changes and elevation have an important effect in altering the incident sunlight angle on solar panels, which affects their power output. Hills, in particular, are prone to high wind speeds, which pose issues to the panels' stability. This instability not only jeopardizes the structural integrity of the panels, but it also raises concerns about the location of both the motor and the panels. As a result, variations in terrain and elevation present difficulties that must be carefully considered when designing and implementing solar tracking systems to ensure optimal performance and reliability.

### 2.1.4 Effect Of Rainfall

In the Bredasdorp, summer conditions occur during the months of December until March. During these months, Bredasdorp experiences average temperatures between 17 – 24 degrees as seen in the figure below [17].

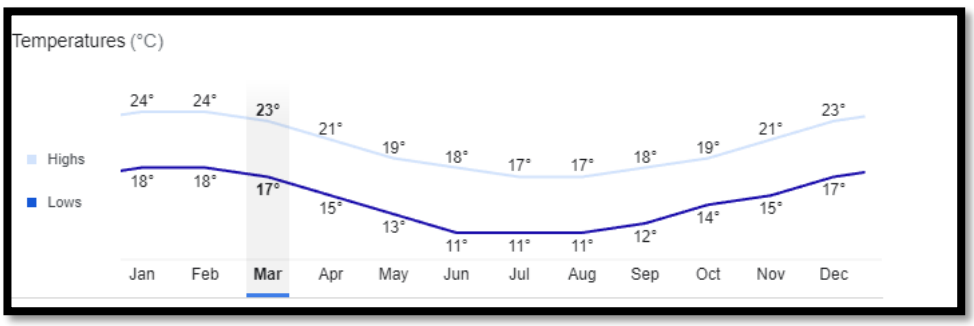


*Figure 3: Average Monthly Temperatures in Bredasdorp [17]*

The area has rainfall levels experienced by Bredasdorp, as depicted in the succeeding figure. December to March generally experience lower precipitation levels compared to the other months [18].

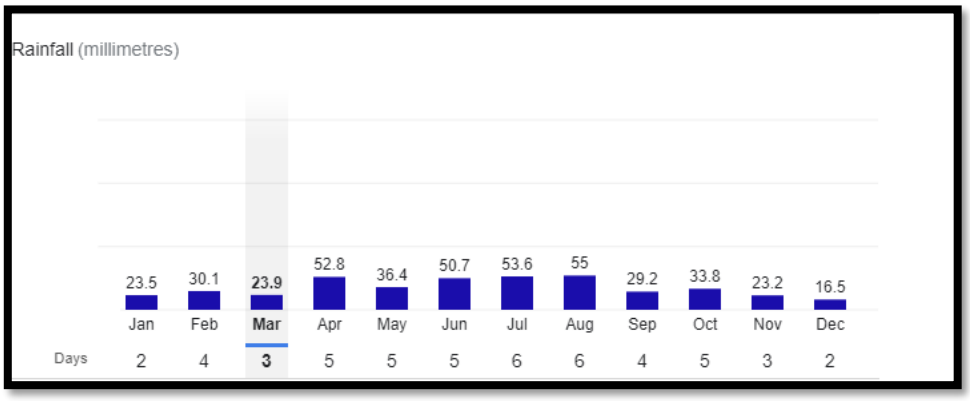


*Figure 4: Average Annual Rainfall In Bredasdorp [18]*

As much as the rainfall contributes to obstructions that minimize the sunlight absorbed by the solar panel, there is a positive effect as the panel accumulates dust over time, reducing the amount of sunlight rays absorbed by the panel, thus rainfall helps clear this for increased sunlight energy absorption. Thus, rainfall will not be used as a disturbance in the model of the solar tracker control system.

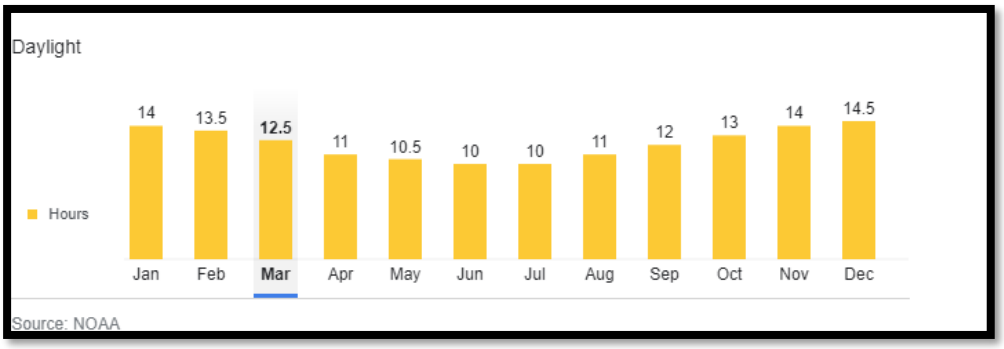


*Figure 5: Average Daylight Received By The Bredasdorp Area [18]*

In the summer, the sun's rays are more potent, reducing the amount of energy absorbed by the panel; however, this is offset by the longer sunshine hours, which compensate for the reflected sun energy that was not absorbed by the panel, as seen in the figure above. Bredasdorp's latitude is around -34.5329 degrees south of the equator. This suggests that Bredasdorp is placed around 34.5329 degrees south of the equator, which will have an impact if the other axis is also considered for analysis [18].

## 2.2 Motor Actuation

The transfer function of the DC motor will be retrieved from existing literature and demonstrated to be well suited for the application after all factors have been considered. The actuation precision will also be important in obtaining accurate results from the model.

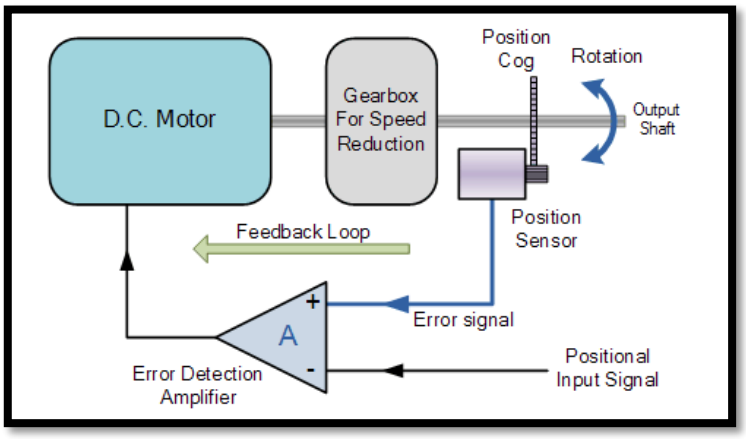


*Figure 6: Block Diagram Of a Servo Motor [12]*

From literature, the accuracy of the servo motor was determined to be ± 0.02 degrees without any load [13]. Thus, Perfect actuation will not be possible due to mechanical tolerances, sensor inaccuracies, and environmental effects and response time. The sun has different positions throughout the year and different weather conditions which affects the tracking accuracy. Mark McDonald suggested that the error of the sun tracker can be determined by the difference between power feedback signal and former signal which concluded that the solar tracker responds late by 0.5 degrees and the servo feedback signal corrects the error by 2.65 degrees [14]

Therefore, the accuracy of the solar tracker is 2.65 degrees [14].

## 2.3 Panel Efficiency

Simply tilting the panel reduces the amount of solar energy collected by the collecting module. As a result, a solar tracker's placement and tilting angle are determined by the height of the site [15]. The tracker collects less energy in both summer and winter due to cloud cover, temperature fluctuations, and altitude changes [15].

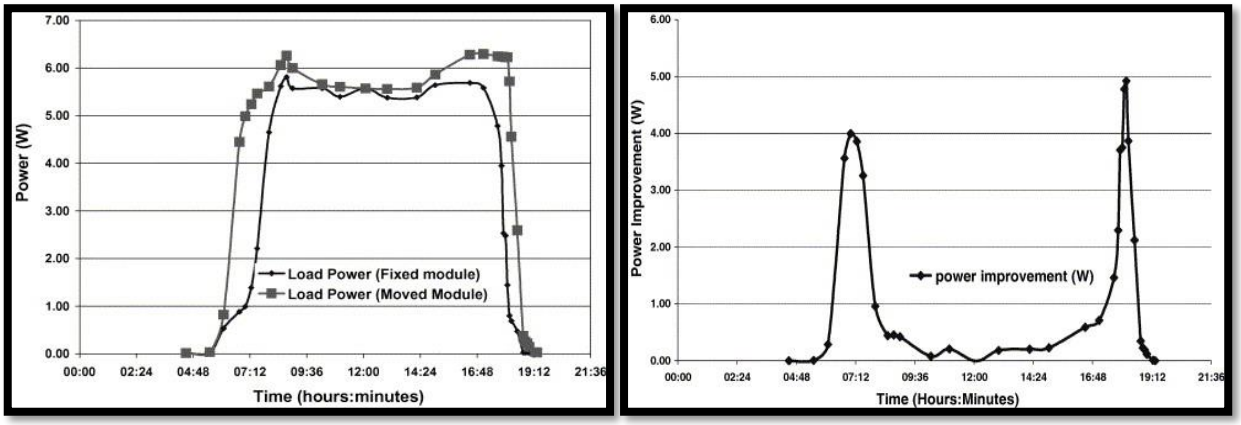


(a) (b)

*Figure 7: Power Output Of Fixed And Tilting Panel [15]*

The data analysis indicates different patterns in the collector's daily energy collection efficiency. Between 06:00 and 08:00, the energy collector has a very high efficiency rate of 66%. However, from 08:45 to 16:30, efficiency drops considerably to 3%, indicating a decrease in energy absorption during this time period. Subsequently, between 16:30 and 18:30, efficiency improves significantly, reaching 45%. The analysis highlights the data' consistency and reliability, with a margin of error of less than ±2%, indicating their accuracy.

## 2.4 Solar Tracking Methods

Photoelectric Sensors are typically placed at the two extreme/outermost ends of the panel, so that they can both measure light intensity. If one of the sensors detects a higher light intensity than the other, the drive module tilts the panel until the perceived light intensity of the sensors is equal (or the error is minimal) [16].

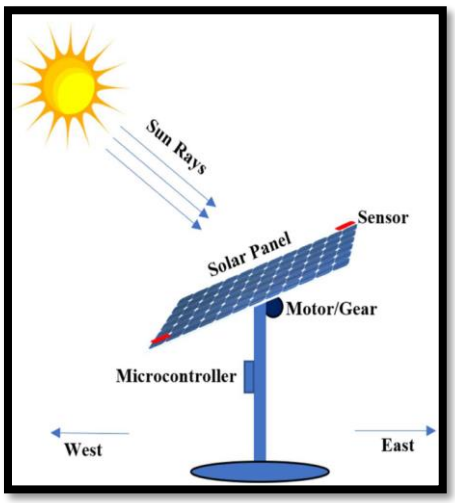


*Figure 8: The working Principle of Photoelectric Sensors for Solar Tracking [16]*

Another method of tracking the sun's position is using algorithms that predetermine the sun's position given inputs such as the latitude and longitude coordinates of the area where the panel is located [16]. For the convenience and accuracy of the model, the latter approach will be used as it requires less maintenance and minimal calibration.

Solar panels are usually installed at an angle to provide optimal irradiation. The direction and angle of this tilt is based on the location of the site, primarily based on the longitude of the installation. Installations in the northern hemisphere should be tilted facing south, and installations in the southern hemisphere should be tilted facing north. The degree of tilt varies according to longitude, generally the longitude of the installation site is a good reference for the angle of tilt. For example, a fixed tilt installation in Sacramento, California, which is at 38.5 degrees North longitude could be facing south and tilted at approximately 38.5 degrees [16].

## 2.5 Zenith And Azimuth Rotation (Dual Tracking)

Zenith and azimuth rotations are fundamental notions in spherical coordinate systems, especially in applications that need accurate orientation and tracking, such as solar trackers. Zenith rotation is the vertical movement of an object around a horizontal axis that represents its distance from the zenith, or the point immediately overhead. This form of rotation is essential for regulating the vertical angle of solar panels so that they capture the maximum amount of sunlight as the sun moves across the sky. Azimuth rotation, on the other hand, refers to horizontal movement along a vertical axis, similar to compass directions (0° for north, 90° for east, 180° for south, and 270° for west). This rotation enables solar panels to follow the sun's horizontal position, ensuring they are always facing the sun directly [35].

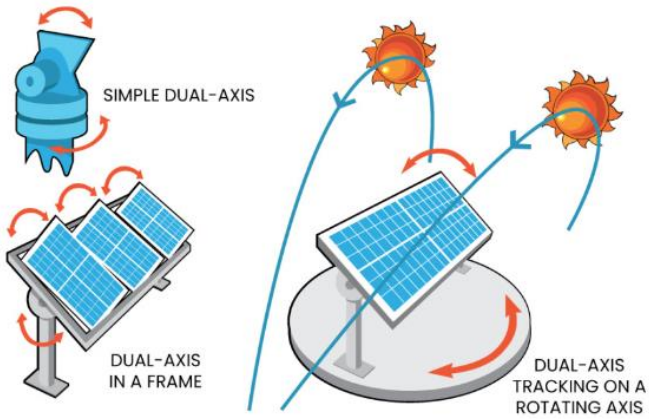


*Figure 9: Dual Solar Panel Tracker [37]*

Dual-axis tracking systems incorporate both azimuth and zenith rotations to provide comprehensive 3D orientation control, significantly enhancing the efficiency of solar panels [36]. By continuously adjusting both the vertical and horizontal angles, these systems can maintain an optimal angle of incidence between the incoming sunlight and the solar panel surface throughout the day and across different seasons. This

dual tracking ensures maximum solar energy absorption, leading to increased energy output compared to single-axis tracking systems, which only adjust in one direction.

When applied to solar trackers, the combination of azimuth and zenith rotations imposes several impacts. Firstly, it increases the complexity and cost of the system due to the need for more sophisticated sensors, motors, and control algorithms. However, the benefits outweigh these drawbacks, as dual-axis trackers can significantly boost the efficiency of solar panels by up to 30-40% compared to fixed systems [37]. This improvement in efficiency results in higher energy yields and quicker return on investment. Additionally, dual-axis tracking systems can adapt to various environmental conditions, maintaining optimal performance even on cloudy days or in less-than-ideal locations. Incorporating both zenith and azimuth rotations into solar tracking systems provides substantial performance advantages, making them a preferred choice for maximizing solar energy capture.

# 3. PERFORMANCE SPECIFICATIONS

## 3.1 General Specifications

A solar tracker is multidisciplinary system consisting of various subsystems integrated harmonically to yield energy from the sun [5]. Performance specifications of a mechatronic system clarify the behaviour, expectations and capabilities of a design contributing to the efficiency of the system [5].

*Table 1: Global Specifications [6]*

| **Description** | **Symbol** | **Values & Units** |
|---|---|---|
| Tilt angles | $\Delta\theta_{tilt}$ | 55° east/west |
| Motor drive | MD | 250 to 370W |
| Posts tolerance | $\Delta y$ | -150mm, +400mm |
| Installation tolerance | It | 50mm, 2 vertically |
| Max. Operational Wind speed | $W_s$ | 20 m/s standard tracking |

## 3.2 Time Domain Specifications

Time domain analysis focuses on determining the Mechatronic system behaviour due to an input and analyse its response function. The analysed system is of first order response which is non homogenous and can be further analysed as a step, ramp and a sinusoid response. The time-domain specifications for the single-axis tilting solar tracker are listed below:

- The **tracking error (Δθ)** is the difference between the actual position of the sun and the orientation of the solar panel, an error of less than 5°(0.087 rad) is desirable [6]. More energy will be harnessed if the error is smaller.
- A shorter **settling time (Ts)** is preferable for the solar tracker, and should be not more than 5 seconds [37].
- The desirable/optimal angular speed of the tracker is estimated to be at least 1°/s (0.017 rad/s) [37].

## 3.3 Frequency Domain

- Bandwidth:

$$Bandwith = \frac{0.35}{settling\ \ time}$$

Using equation above, the bandwidth must be at least 0.875 dB

# 4. MODEL DEVELOPMENT

## 4.1 Assumptions

- Panel mounting and tracker are rigid bodies
- Constant wind speed
- Uniform mass and/or mass moment of inertia
- Motion constraint to 2D (single axis)
- Solar panel made out of crystalline silicon and PV cells
- Solar panel connected to the centre of mass of tracker (mass concentrated about pivot point)

## 4.2 Generalised System Coordinates

The figure below depicts the single-axis solar tracker's free-body diagram, as well as the forces and moments operating on it.

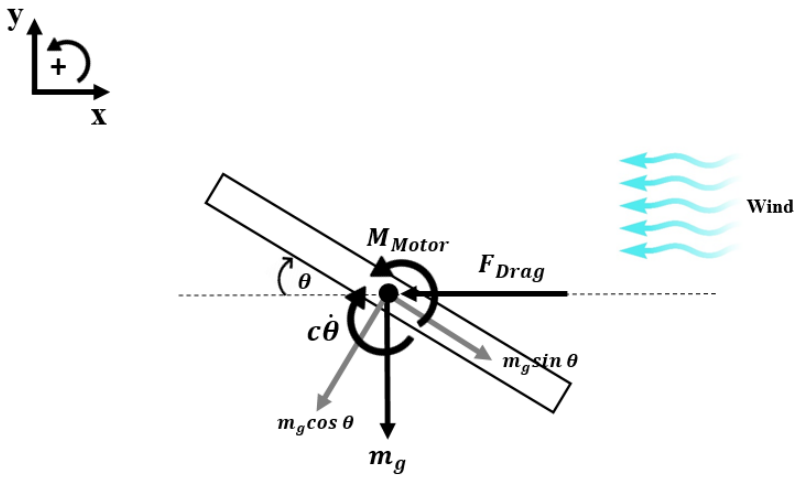


*Figure 10: Free-body diagram of the single axis solar tracker*

## 4.3 Development Of The Model

To enhance comprehension and streamline the model's development process, the model will be categorized into three stages: the physical (prototype) model, the analytical (mathematical) model, and the numerical (computer) model. This sequential technique allows for effective debugging by tracking each stage individually, making it easier to identify possible errors as they develop.

### 4.3.1 Physical Model (Prototype)

The prototype configuration entails using the motor to rotate the tracker and aligning the panel with sunlight rays to increase efficiency and solar energy absorption. Figure 3 depicts the prototype's configuration, including the tracking direction built specifically for usage in the southern hemisphere.

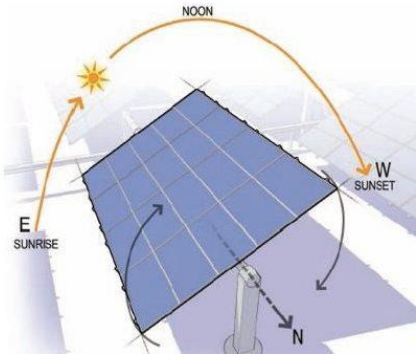


*Figure 11: Physical Setup Of The Solar Panel And Tracker [7]*

### 4.3.2 Analytical Model (Mathematical)

The derived equations have values that can be substituted after the derivation, it is preferred that the derivation is done using variables to track progress and less complexity. The variable specification parameters are in the table below:

*Table 2: Mathematical Modelling Variable Specifications*

| | |
|---|---|
| $\boldsymbol{c(motor)}$, $\boldsymbol{kg.m^2/s}$ | 0.1 |
| $\boldsymbol{c(panel)}$, $\boldsymbol{kg.m^2/s}$ | 0.3 |
| $\boldsymbol{k}$ | 0.14 |
| $\boldsymbol{J}$, $\boldsymbol{kg.m^2}$ | 4.108867 |
| $\boldsymbol{I_m}$, $\boldsymbol{kg.m^2/s^2}$ | 0.01 |
| $\boldsymbol{F_D, N}$ | 21.94648 |
| $\boldsymbol{l, mm}$ | 40 |

#### 4.3.2.1 Mechanical Model Specifications

To facilitate navigation and understanding of equation flow, only final equations are examined; the derivation method is detailed in the appendices. The nonlinear equation is obtained by analysing mathematical equations from the solar panel tracker FBD in figure 9, to linearize the equation, small angle approximation is used.

**Non-Linear Equation:**

$$J\ddot{\theta} = \frac{k_t(V_a - k_e\dot{\theta})}{R} - c\dot{\theta} - wl\sin\theta + F_D l\cos\theta$$

**Linearized Equation:**

$$J\ddot{\theta} = \frac{k_t(V_a - k_e\dot{\theta})}{R} - c\dot{\theta} - wl\theta + F_D l$$

Formulation of the motor equations is all in terms of variables, the table below lists the numerical values of the variables for calculation:

*Table 3: Mechanical Model Values*

| | |
|---|---|
| $\boldsymbol{c,\ kg.m^2/s}$ | 0.1 |
| $\boldsymbol{k_t, Nm/A}$ | 0.14 |
| $\boldsymbol{J,\ \ kg.m^2}$ | 4.108867 |
| $\boldsymbol{I_m,\ kg.m^2/s^2}$ | 0.01 |
| $\boldsymbol{F_D, N}$ | 21.94648 |
| $\boldsymbol{l, mm}$ | 40 |

### 4.3.2.1 Electrical And Mechanical Motor Model Specifications

The idea to use a DC armature driven electric motor originated from the fact that direct current provides faster response times than alternating current and may be powered directly from a battery without the need for extra components such as an inverter. However, because the movement will be limited, the DC will be connected to a gearbox, which will limit the angle and rotation speed. Figure 11 displays the electric circuitry for the chosen motor.

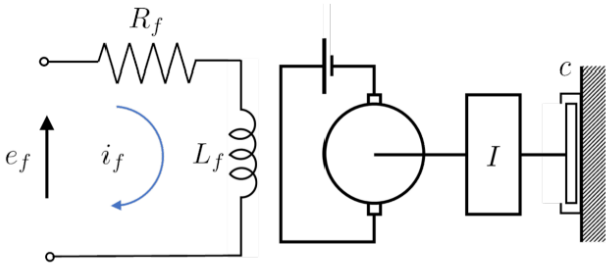


*Figure 12: Armature Controlled DC Motor [19]*

Below are the related equations [19]

$$V_a = R_{i,a} + L\frac{di,a}{dt} + V_{em} \quad (1)$$

$$V_{em} = k_e\theta \quad (2)$$

The equation below represents the mechanical part of the motor:

$$J_m\ddot{\theta}_m = T(t) - \ c\dot{\theta}_m \quad (3)$$

$$T(t) = kt_{ia} \quad (4)$$

The torque equation if further simplified into:

$$T(t) = \frac{kt(V_a - k_e\dot{\theta})}{R}$$

Formulation of the motor equations is all in terms of variables, the table below lists the numerical values of the variables for calculation:

*Table 4: Armature Motor DC specifications*

| | |
|---|---|
| $\boldsymbol{c,\ kg.m^2/s}$ | 0.1 |
| $\boldsymbol{k_t, Nm/A}$ | 0.14 |
| $\boldsymbol{k_e, Nm/A}$ | 0.934 |
| $\boldsymbol{R, \Omega}$ | 2.5 |
| $\boldsymbol{L, mH}$ | 70 |
| $\boldsymbol{V_e, V}$ | [-12, 12] |

#### 4.3.3.4 Representation Of The Solar Tracker In State Space

$$\frac{d}{dt}\begin{bmatrix}\theta \\ \dot{\theta}\end{bmatrix} = \begin{bmatrix}0 & -0.08375 & -2.0060 & 0 \\ 0 & 1 & 0 & 0\end{bmatrix}\begin{bmatrix}\theta \\ \dot{\theta}\end{bmatrix} + \begin{bmatrix}1 \\ 0\end{bmatrix}V$$

$$y = [0 \quad 0 \quad 0.14 \quad 0]\begin{bmatrix}\theta \\ \dot{\theta}\end{bmatrix}$$

Where,

$$\frac{d}{dt}x = Ax + Bx$$

### 4.3.3 Numerical Model

A solar tracker is a mechatronic system which rely on synthesis and can be categorized based on time and model linearity. The closed loop control system is composed of elements which sum up to the operations of the while system including the reference input element, controller element, actuator, process which is affected by the disturbance input element and a response through feedback element detected by a controlled sensor [20]. For the uncontrolled system, the methodology is analysed by interpretation of time and frequency domain plots. The interpretation is utilized to determine the performance of the system and closed loop stability for the uncontrolled systems.

The block diagram below depicts an uncontrolled system and is used for system analysis and data extraction for system interpretation.

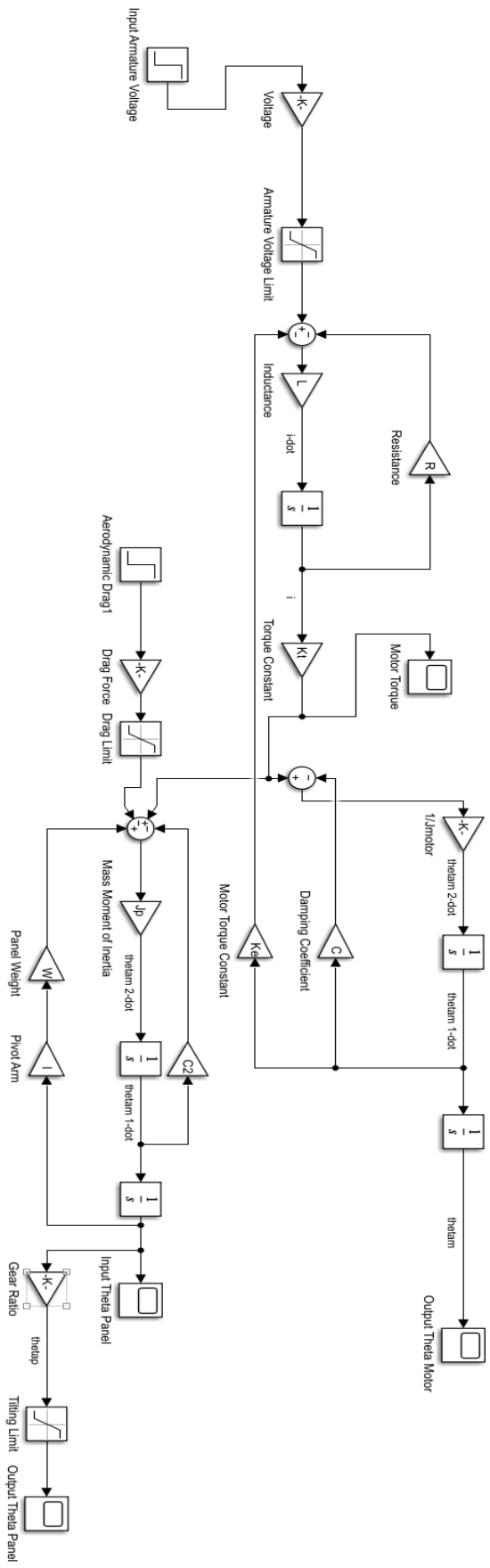


*Figure 13: Uncontrolled Plant Block Diagram (Simulink)*

### 4.3.4 Uncontrolled System Response

#### 4.3.4.1 Time Domain

Time-domain performance specifications includes the transient response of the system which are time base and vary between the step, Ramp, Impulse, and the Sinusoid response. If the system is linear, the principle of superposition enables the consideration of the response to input commands rather than the response from external disturbances. In the system being analysed the disturbance inputs were from the input commands which was the voltage, since there is no sensor included, the system is an open loop which tracks the position of the sun. There are two disturbances for the uncontrolled system which is the voltage and aerodynamic drag as illustrated in figure 1and 2 below. For voltage the response function was restricted to strictly operate within [-12, 12] limit and drag was bounded within [-21.95, 21.95] limit which was dictated by the motor specifications and the panel design constraints.

#### 4.3.4.2 Input Disturbances (Voltage)

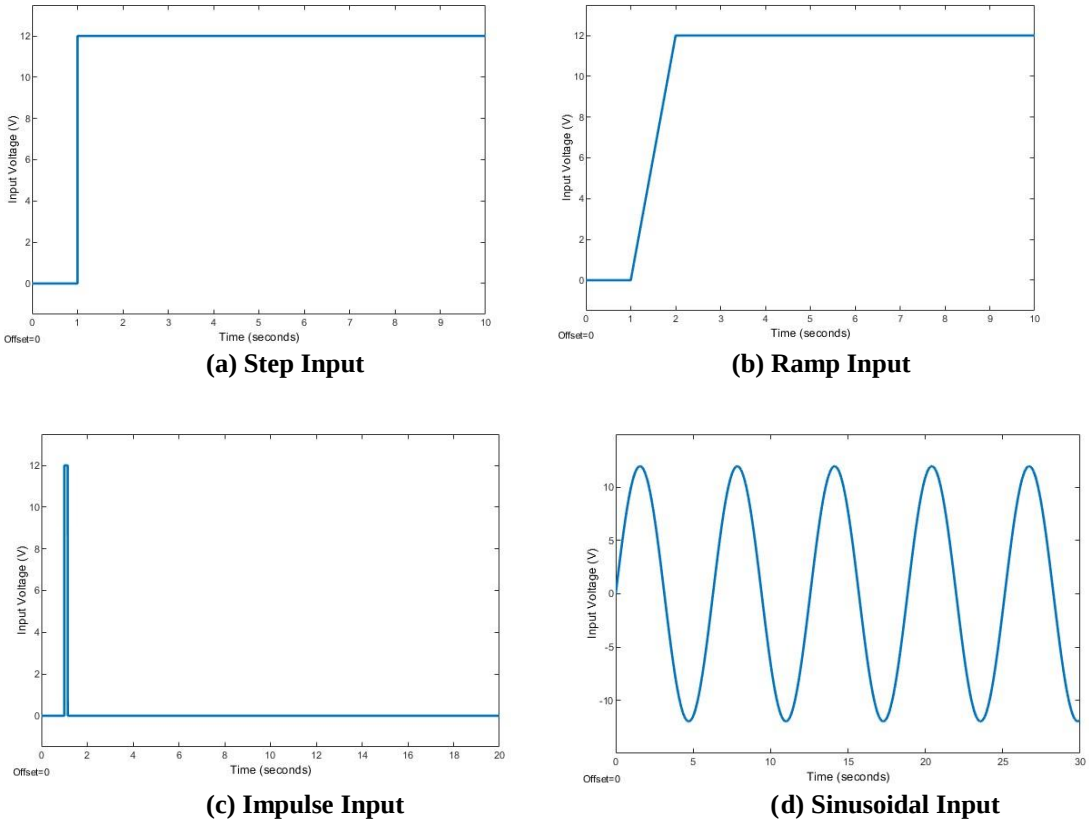


**(a) Step Input** **(b) Ramp Input**

**(c) Impulse Input** **(d) Sinusoidal Input**

*Figure 14: Voltage Input Disturbances Affecting The Uncontrolled Plant*

4.3.4.3 Input Disturbances (Drag)

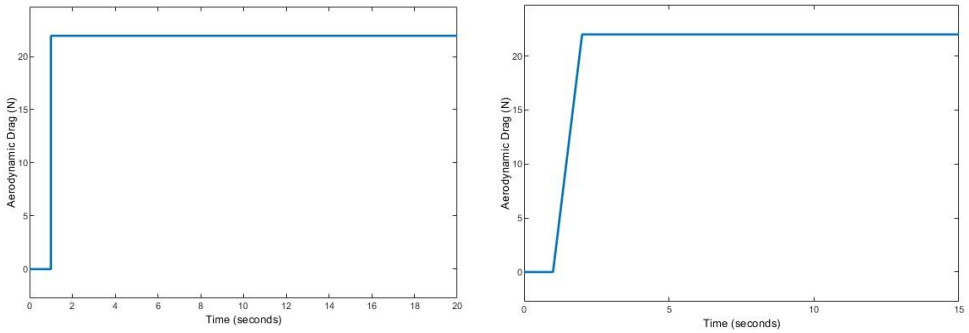


**(a) Step Input** **(b) Ramp Input**

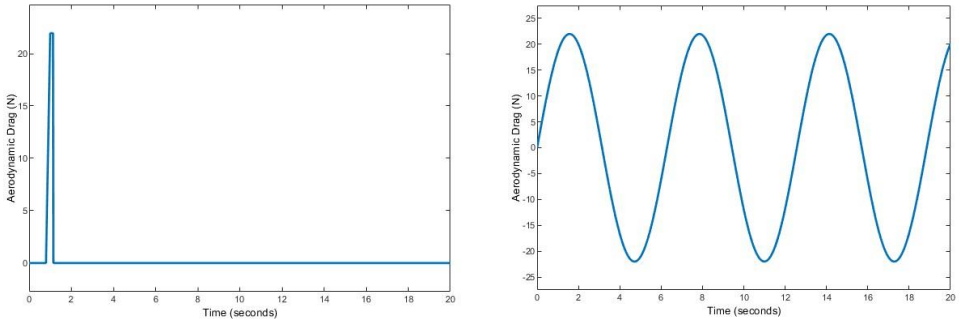


**(c) Impulse Input** **(d) Sinusoidal Input**

*Figure 15: Drag Input Disturbances Affecting The Uncontrolled Plant*

The input voltage disturbance signals a positive signal to the system which suggest that the motor will rotate in the clockwise direction and thus driving the panel from east tilting to the west to follow the location of the sun. During sunset the panel's tilt angle will reach its limit and a negative signal from the input voltage will produce a negative tilt angle which would return the panel to its initial position which is in the east direction in order to prepare for sunrise, which is expected to rotate counter-clockwise.

4.3.4.4 Time Responses

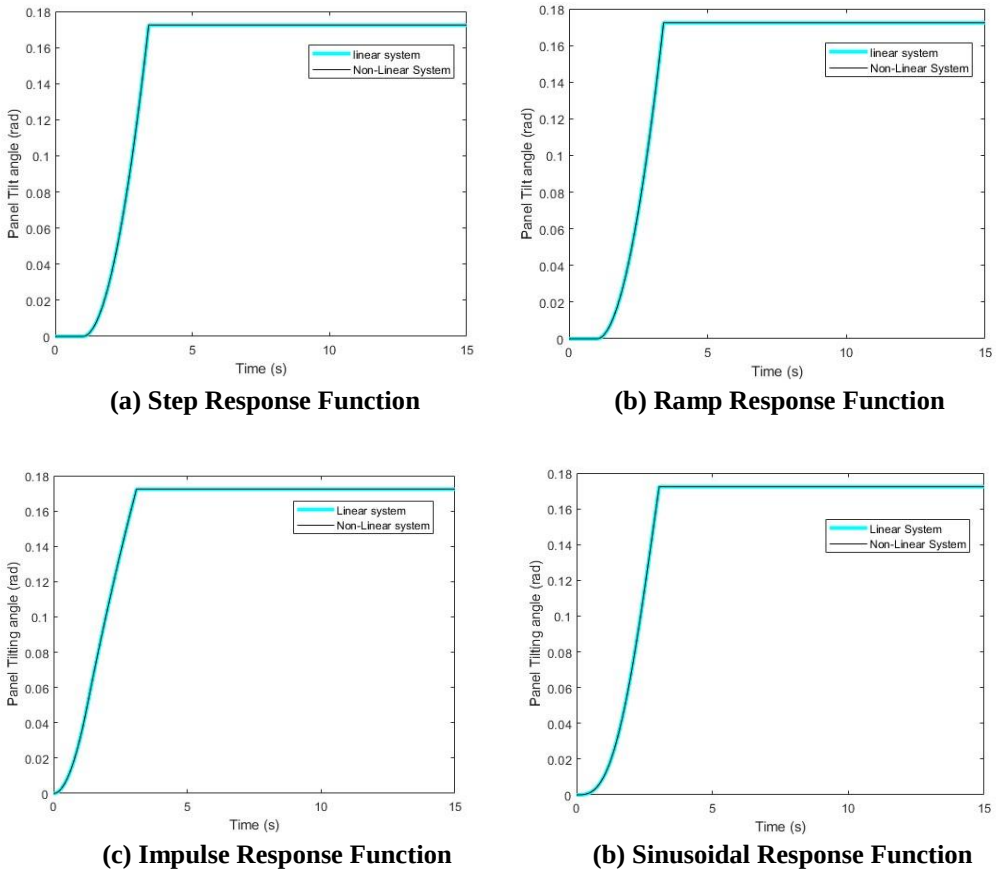


**(a) Step Response Function** **(b) Ramp Response Function**

**(c) Impulse Response Function** **(b) Sinusoidal Response Function**

*Figure 16: System Response Functions*

As illustrated by Figure 15 above, the input disturbance from both the voltage and drag input reacts to almost similar output response plots for both the linear and non-linear response due to time-domain performance specifications. There is less error detected in the response resulting from the linear and non-linear plots as illustrated by Figure 15 above. The results shows that the linearization equation developed through the small angle approximation was valid and was suitable for the solar tracker system. From the data obtained in the plots the there is a 0.67% error between the two systems. The tilting angle step was limited to 0.1724 radians, for angles larger than the limit, the non-linearized system results in higher angles than the linearized system but the error is not evident due to the limit of 0.1724 radians at 3.04 seconds.

Assuming that a positive polarity of the amateur voltage was applied relative to the DC motor winding configuration. A positive signal was applied to the motor, and the motor turned the panel in the clockwise direction from the east. The motor will turn the panel from sun rise till sunset by following the Location of the sun, after sun set, the panel will continue due to using an uncontrolled open loop system therefore the system will not stop after sunset. The system cannot determine when sunset is reached at 1.91 radians therefore, the panel will rotate continuously, which will misalign with the sun.

The step and ramp function results in a response that is 1 second later than the impulse and a sinusoidal response but arguably follows the same slope and output the same tilt angle of 0.1724 radians. The ramp response is time variant but the effect is evident after 0.1724 radians which behaves similar to a step function, the impulse function reacts quicker than all the transient responses due to occurring at a smallest time which represents the sudden shock due to wind and voltage disturbances. At zero up to one the sinusoidal function produced a minor sin wave then followed the same slope as other responses. The drag and the weight of the panel makes it difficult for the panel to balance which makes the slope of the responses high, which suggests that the specified operating conditions were not satisfied.

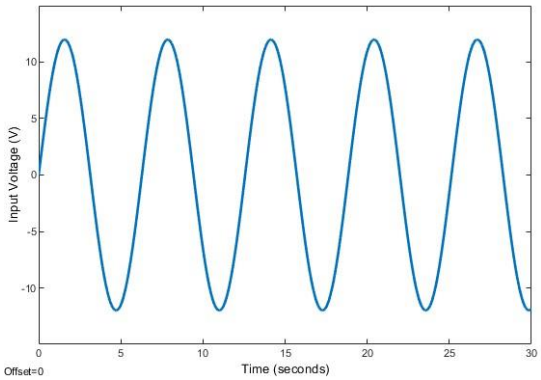


**(a) Bounded Input Voltage**

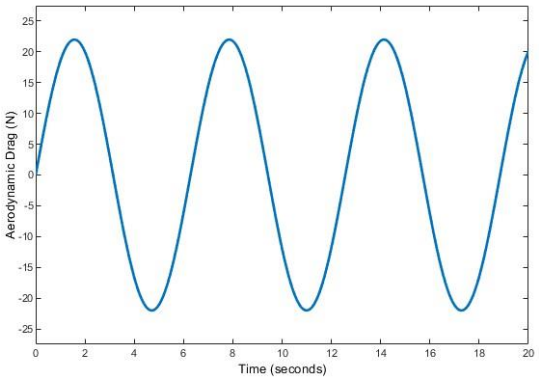


**(b) Bounded Input Drag**

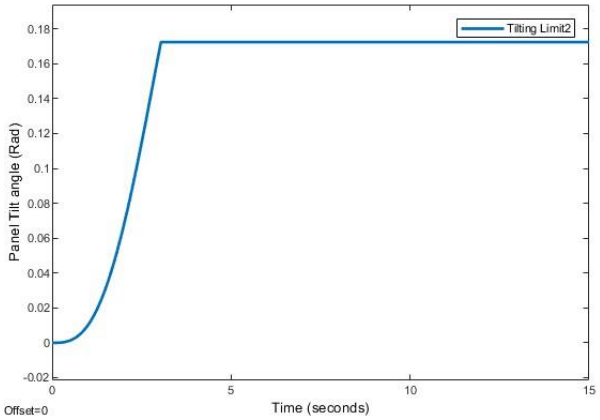


**(c) System Response To Bounded Inputs**

*Figure 17: Bounded System Response*

Bounded input and bounded stability analysis were used to evaluate the stability of the non-linearized systems because such systems exhibit complex behaviour as a function of time. This analysis suggests that if limits are bounded to the signal the output should also follow the same logic in order to maintain model stability [21].A sinusoidal disturbance armature voltage input was utilized with was bounded from -12V to 12V in order to account for motor specifications and rotational displacement. Another sinusoidal drag input disturbance was bounded in the [-21.94, 21.94] N wind drag range as per panel specifications. The response is unbounded since it continues until infinity and was stopped by an angle limit after reaching the step of 0.1724 radians in 3.04 seconds which does not guarantees that the output remains within the specified bounds throughout the duration as illustrated in

figure 4 above. The system is unstable which goes against the fact that the real part of the poles of the transfer function are both negative which suggests that the system is stable [21].

#### 4.3.4.5 Uncontrolled System Interpretation

The system's detailed analysis covered above suggests that the uncontrolled system is partially stable as proven by the bounded input bounded output criteria, therefore a system controller is required in order to achieve main aim which is tracking g the location of the sun. The Controller is broken into subsections, namely the Root Locus and the Proportional Integral Derivative (PID) controller, which are techniques employed to understand the be behaviour of the system's poles and regulate the systems output through continuous adjustments of the input disturbance based on the error reading and the desired system's output as to fully develop a suitable control system for the tracker [22].

#### 4.3.4.6 Frequency Domain (Bode Plot)

Bode plots help provide a clear visual representation of the system's frequency response, demonstrating how the magnitude and phase respond to various frequencies of input signals. This helps in understanding how the system will perform under various operating situations. Bode plots, also look at the gain and phase margins, which are useful for assessing the stability of control systems. The robustness of the system against fluctuations and disturbances is indicated by the gain and phase margins. Insufficient margins can cause the system to oscillate, become unstable, or even become difficult to control. A lower bandwidth typically results in a slower system response.

The open-loop transfer function below was used to generate the bode plots:

$$\frac{\theta(s)}{V(s)} = \frac{0.1366}{s^2 + 1.475\,s + 1.9566}$$

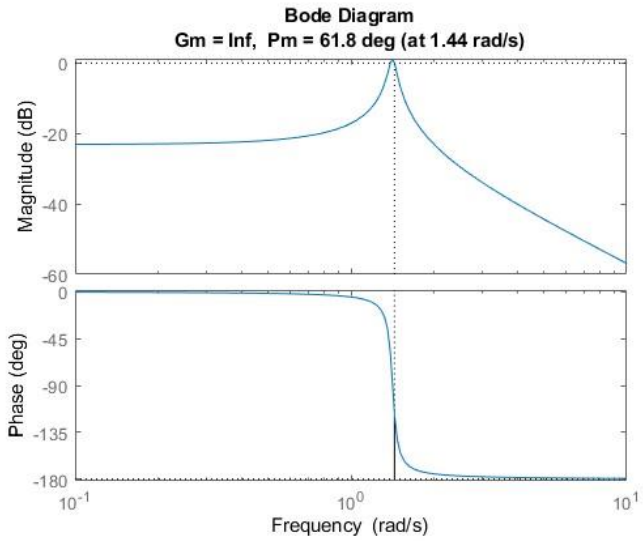


*Figure 18: Uncontrolled System Bode Plot*

For the solar tracker system to precisely track the sun's movement throughout the day, stability is essential. Given that the gain margin typically indicates how much the gain of the system can be amplified before it becomes unstable. An infinite gain margin observed in Figure 17 above, ensures that the system will stay stable even in the event of fluctuations in its gain, such as variations in the amount of sunlight or mechanical wear over time. This stability guarantees that there are less oscillations or instability problems in the solar tracker system's continuous operation. However, it is not possible to infinitely increase the gain, as the system's components have limitations in general. For instance, the DC motor can only take 12V and there is a maximum torque that it can generate for actuation. Additionally, an increase in the gain is likely to make the system sensitive to noise which can reduce its performance, leading to instability.

A observed from figure 17, the system may withstand an additional 61.8° of phase shift before reaching the stability threshold, which is typically 180 degrees for stability. The system's phase response is reasonably distant from the instability region if it has a phase margin of 61.8°. Which implies that the system can withstand fluctuations or disruptions without experiencing significant instability.

Using MATLAB, the bandwidth was determined to be 2.1982dB. The bandwidth is marginal. However, given that the change in the sun's position per unit second is relatively low, this bandwidth is reasonable since the system will not have to respond for every second of change in the sun's position.

### 4.3.5 System Stability Analysis

System stability is a vital indicator of a system's robustness since it guarantees that the system will reach its equilibrium points following the introduction of a disturbance. While there are several ways to analyse stability for a linear time invariant system, only the Routh-Hurwitz criterion, Nyquist stability, and the pole and zero criteria were taken into consideration. Considering that the non-linear system is time-variant, only the bounded input, bounded output criteria applied.

#### 4.3.5.1 Routh-Hurwitz Criterion

The Routh-Hurwitz Criterion is used to examine the stability behaviour of the closed loop system by determining how many roots of a polynomial in $s$ are in the right half of the $s$-plane, the left half of the $s$-plane, and on the imaginary axis.

Characteristic equation for the model is given by:

$$s^2 + 1.475s + 1.9566 = 0$$

Given that the coefficients of the equation are non-zero and positive, we can almost conclude that the system is stable. However, this is not enough information as the roots may be complex. We thus construct the Routh table to find the number of roots in the right hand side of the s-plane.

*Table 5: Uncontrolled system Routh table*

| | | |
|---|---|---|
| $s^2$ | 1 | 1.9566 |
| $s^1$ | 1.475 | 0 |
| $s^0$ | 1.9566 | |

Since every element in the Routh table's initial column has the same sign, according to Routh-Hurwitz criterion the system is stable.

### 4.3.5.2 Pole-Zero Plot

The pole-zero map provides insights into the dynamic behaviour of a system. Poles represent the roots of the system's characteristic equation.

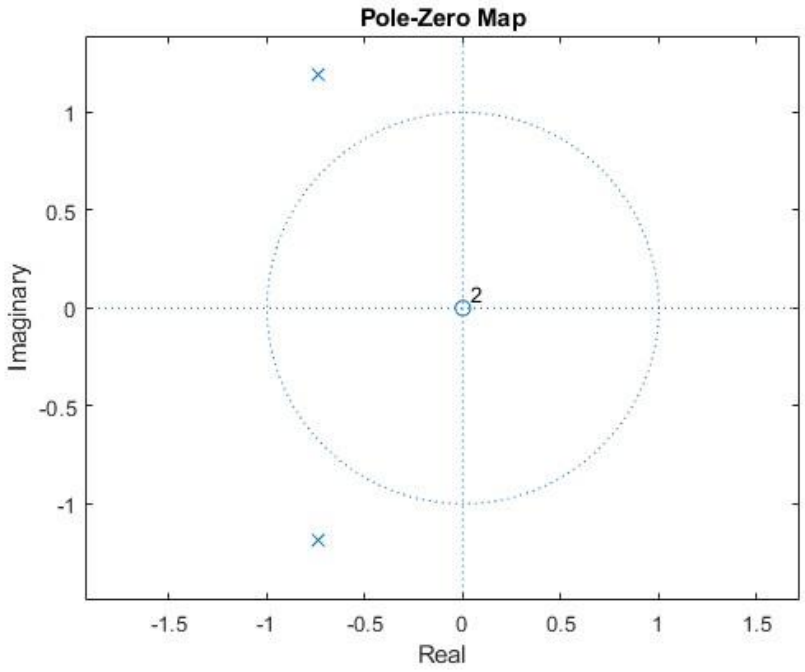


*Figure 19: Uncontrolled system pole-zero map*

As depicted in figure 18, all the poles are in the left hand side of the s-plane.When all poles are in the LHP, the real parts of their complex conjugate pairs are negative, indicating that any transient response will decay over time and not grow uncontrollably.

### 4.3.5.3 Nyquist Stability Analysis

Nyquist plots are used in control system analysis to visualize system frequency response in the complex plane. They evaluate stability by examining if the plot encircles the (-1,0) point in a counter clockwise direction. In simple terms, To ensure stability, the plot should not include the (-1,0) point of 1 gain crossover frequency. If (-1,0) is enclosed, it should be counter clockwise. This process helps in understanding system behaviour and stability standards.

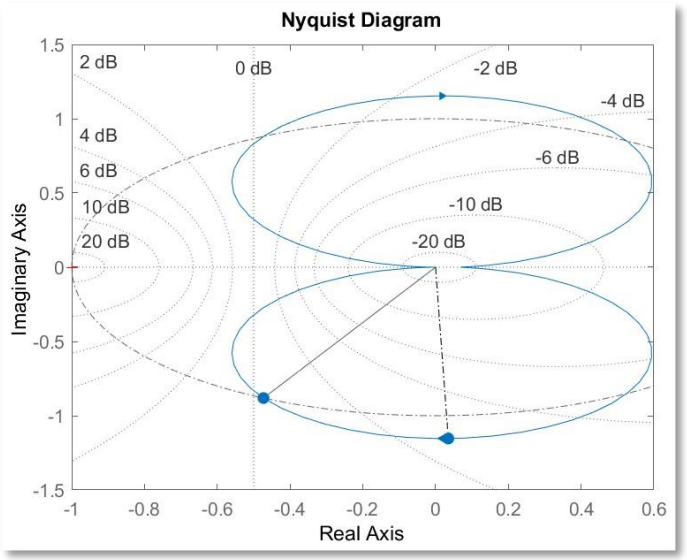


*Figure 20: Nyquist Stability Plot*

The stability of the system is confirmed by observing that the Nyquist plot does not enclose the (-1, 0) point in a clockwise direction, adhering to the stability criterion. By complying with this criterion, the system demonstrates robustness against instability and ensures predictable and reliable performance in solar tracker real-world applications. Therefore, the absence of clockwise encirclement reaffirms the system's capability to maintain stability under varying operating conditions, validating the effectiveness of the control strategies employed in its design.

### 4.3.5.4 Phase and Gain Margin (Relative Stability Analysis)

Relative stability analysis primarily relies on the Nyquist plot, which is named after the (-1,0) crossover frequency that indicates instability. This approach takes into account two crucial parameters: phase margin and gain margin. The phase margin represents the least phase angle prior to the Nyquist plot encompassing the (-1,0) point, whereas the gain margin reflects the minimal gain prior to such enclosure. Stability requires positive values for both phase and gain margins. Furthermore, greater phase and gain margins boost a system's robustness, emphasizing the significance of adequate stability margins in guaranteeing system resilience and performance consistency.

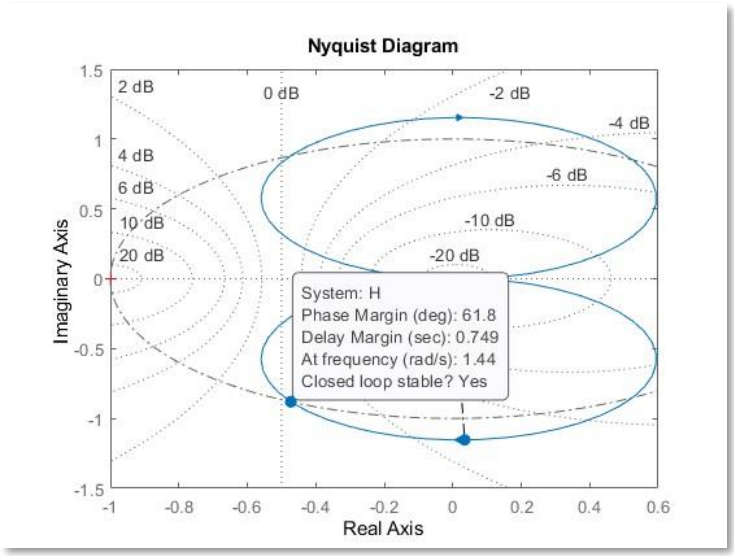


*Figure 21: Relative Stability Plot*

The data displayed in the preceding figure indicate that the system under examination, indicated as 'H', has relative stability characteristics. The phase margin of 61.6 degrees implies that the system has a significant amount of phase angle before the Nyquist plot encircles the crucial (-1,0) point, indicating robustness against oscillatory behaviour and stability. Moreover, the delay margin of 0.749 seconds at a frequency of 1.44 radians per second contributes to the system's stability, suggesting that it can withstand a given amount of time delay without losing stability. The demonstration that the closed loop is stable strengthens the analysis by demonstrating that the system performs consistently within the defined stability margins.

# 5. DESIGN OF A CONTROLLER

In mechatronics engineering, a controller is a device or algorithm that manages the behaviour of a system by adjusting its inputs based on feedback to achieve desired performance and stability. Controllers process error signals, which are the differences between desired set points and actual measurements, to minimize deviations and maintain system performance. When applied to an initially uncontrolled system, a controller will significantly enhance its performance by ensuring accurate and stable operation, improving response times, reducing oscillations, and compensating for disturbances and uncertainties. This results in a more reliable and efficient system that meets specific performance criteria.

## 5.1 The Proportional Integral Derivative (PID) Control Method

Among the various control methods available, the PID controller typically stands out due to its robustness and simplicity. In this case, the PID controller is needed to adjust the position of the solar panels by computing the error between the desired and actual positions, and then employing corrective actions based on proportional ($K_p$), integral($K_t$), and derivative ($K_i$) terms. This results in precise and responsive tracking, enhancing the overall solar energy capture.

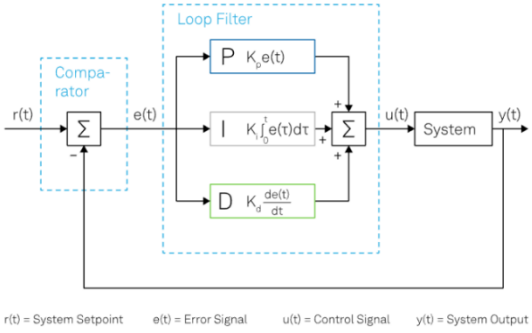


*Figure 22: Sourced PID controller diagram [23]*

The figure above illustrates a sourced typical PID controller where r(t) is the input through a comparator then followed by a loop filter which features the PID and can be broken down as follows, Proportional gain, integral gain, and derivative gain.

Figure 22 below shows the Simulink block diagram of the PID controller used for the uncontrolled system:

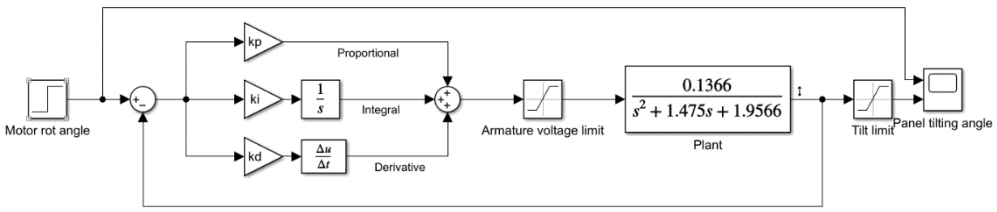


*Figure 23: PID Controller Of The For The Uncontrolled System*

A step input using a tilt angle of 0.078 was inputted in the controller. Since, linearized models often work with small angle approximations, this angle is sufficiently small to fit the approximation. Using the PID tune function on MATLAB, the following PID values were obtained: $K_p = 29.3$ , $K_i = 24.2$ and $K_D = 8.86$ . The resulting response of the PID controller is shown in Figure 23 below.

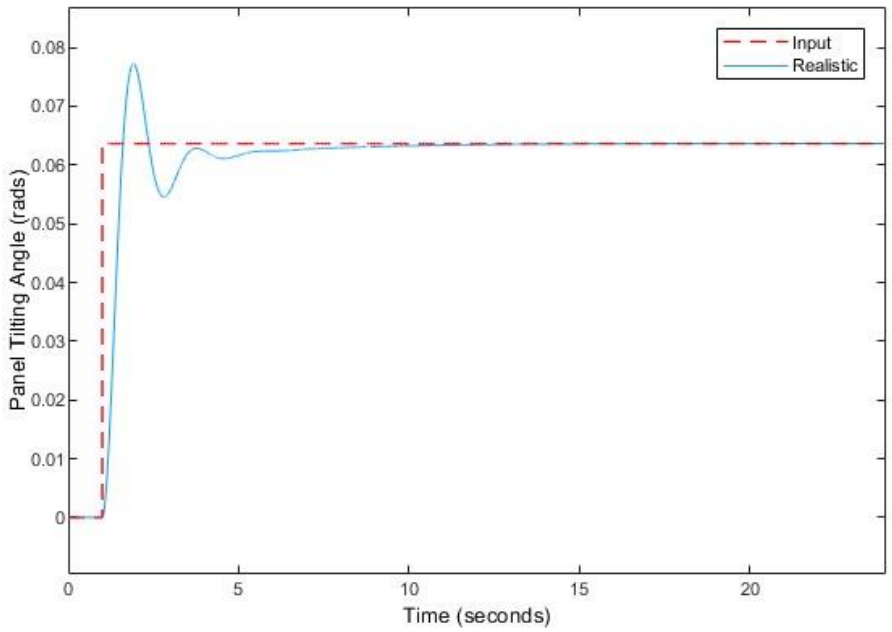


Figure 24: Step input response of the PID controller

The table below shows the comparison between the desired gains and the PID controller gains. A MATLAB function "pidtune" was used to obtain the Kp = 300, Kt = 250 and Ki = 100 values of the PID controller. The resulting specifications are listed in table 1 below.

*Table 6: PID Controller Gains Specifications*

| Specification | Desired outputs | PID outputs |
|---|---|---|
| **Bandwidth (Hz)** | >0.875 | 2.75 |
| **Peak (rad)** | ≤1.2 | 0.082 |
| **Peak time (s)** | <5 | 1.42 |
| **Percentage Overshoot (%)** | <20 | 16.9 |
| **Percentage Undershoot (%)** | <20 | 0 |
| **Steady state error (%)** | ≤5 | 2.01 |
| **Rise Time (s)** | ≤0.4 | 0.264 |
| **Settling time (s)** | <5 | 3.06 |

In figure 23 above, it can be observed that the steady state error is sufficiently small, with a value of 2.01%, this is less than the maximum threshold value of 5%. Moreover, the settling time was found to be 3.06, which meets the desired settling time value of less than 5.

### 5.2 PID controller model simulation

To check if the single-axis tracker model works well in tracking the solar position. The following conditions were used to generate the solar position input to the model:

*Table 7: Summer And Winter Conditions Used To Generate Sun Position Signal*

| | **Summer** | **Winter** |
|---|---|---|
| **Time of the day** | Full 24-hour period | Full 24-hour period |
| **Local latitude** | -34.5439º | -34.5439º |
| **Local longitude** | 20.1360º | 20.1360º |
| **Month** | December | June |
| **Day** | 21 | 21 |
| **Declination angle** | -23.4498º | -23.4498º |
| **Slope of Bredasdorp** | 0 º | 0 º |
| **Solar Altitude angle** | 78.91º | 32.01º |

In the southern hemisphere, where Bredasdorp is located. Typically, the month that experiences the most solar radiation during summer is December, during the solstice period. Hence, December conditions were used. While June experiences the most solar radiation for winter during the solstice period [24]**.** The slope of the chosen site at Bredasdorp was assumed to be 0º, given that the area is at sea level

A MATLAB code was used to generate the position of the sun at 1-hour intervals throughout the 24-hour period. The signal builder was used to map out the change in the elevation angles of the sun and used an input function into the controller model. However, before the solar angles are fed into the model, they must be converted by a potentiometer into voltage values that can then be fed into the DC motor to enable actuation. The potentiometer uses equation 1, as seen below to convert the sun position angles to voltage:

$$V_{out} = V_{tot} \cdot \frac{\theta_s}{\theta_m} \tag{11}$$

**Where;**

$V_{out}$ = The voltage fed into the DC motor, converted from solar angle.

$V_{tot}$ = The total voltage that the DC motor can handle (12V in this case).

$\theta_m$ = The maximum tilt angle of the solar panel (180 degrees).

$\theta_s$ = The elevation angle of the sun at that instant (i.e., during that hour).

Additionally, figure 24 below sows the solar angle input function which models the hourly change in the angular position of the sun:

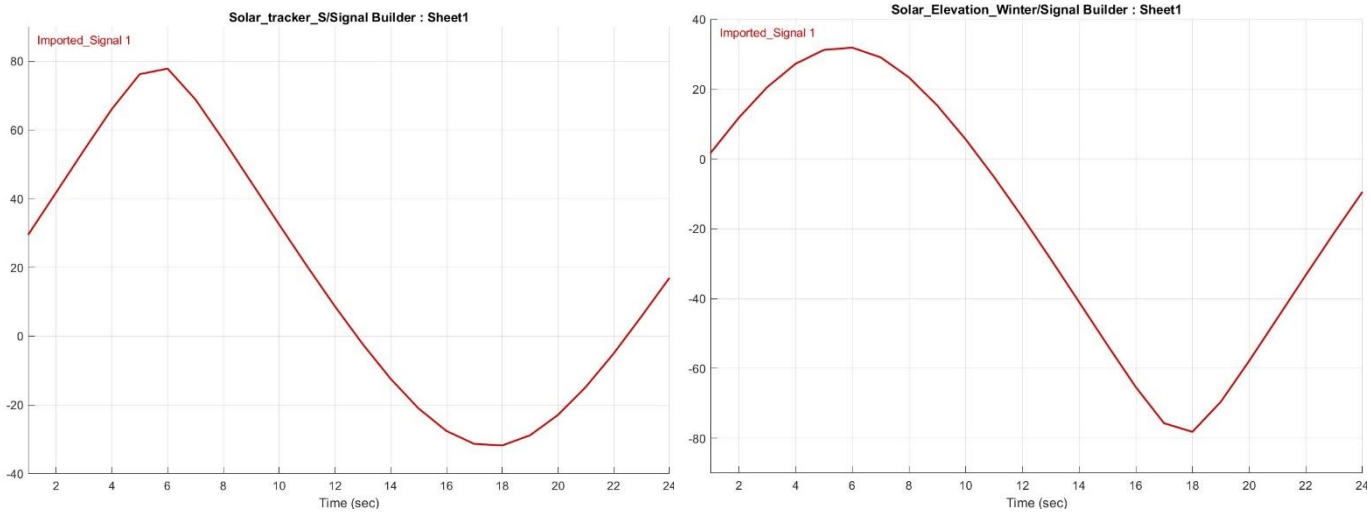


(a) Summer (b) Winter

*Figure 25: Sun Position During a 24-hour Period*

The behaviour of the sun is slightly different in summer than in winter, as displayed in figure 24 above. The model must be able to track and follow these angles as close as possible. The solar positions in figure 24 above were then used as inputs in the controller model shown in figure 22 above. The resulting response from the solar panel is displayed in figure 25 below.

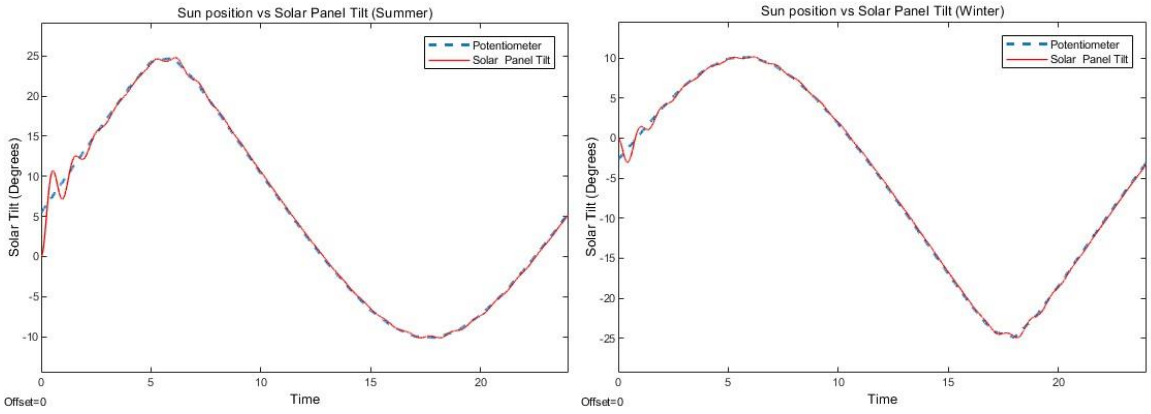


(a) Summer Conditions (b) Winter Conditions

*Figure 26: Solar Panel Tilt Response Relative to the Sun's Position*

Figure 1 show the solar panel tilt angle as compared to the potentiometer readings for sun tracking. At around 06h30 in the morning sun rise is expected as suggested by figure 1, the panel tilts from 25 degrees following the sun throughout the day up to -10 degrees at approximately 18h00 where sun set is expected. During the day from 06h30 up to 18h00 a small error is experienced between the potentiometer readings and the panel tilting angles which suggest that the panel is properly following the sun. From 18h00 up to 23h59 the panel is returning back to

its original position in order to repeat the tracking procedure. From 00h00 up to 06h30 the panel experience instabilities mainly due to aerodynamic drag experienced during the night but PID fine-tuned the instabilities around 04h00 which repeats the process for the whole summer. As suggested by literature, the solar sun tracker is efficient in winter than in summer, Similarly, sun rises around 07h00 in winter and sets around 18h00, as illustrated by figure 2 above, at sun rise the panel starts at 10 degrees and follows the sun throughout the day up to a maximum of -25 degrees at sunset, which suggests that the controller conditions in winter are different in summer, as the sun's location is different relative to the karoo. After 18h00 the panel tilts back to its initial conditions at the same rate up until sunrise of the preceding day until winter is over.

### 5.3 The Root Locus Technique

In control systems engineering, the root locus methodology is a graphical tool used for analysing the movement of the roots of a closed-loop system's characteristic equation on a pole-zero map. By using various control mechanisms, this technique makes it possible to fine-tune controllers such as PID and PDF controllers. Within the root locus structure, the PID controller with realistic gains functions as the plant under examination in the given situation. Figure 25 shows the block diagram exhibiting the root locus technique, which makes the behaviour and stability features of the system easier to see and comprehend [25].

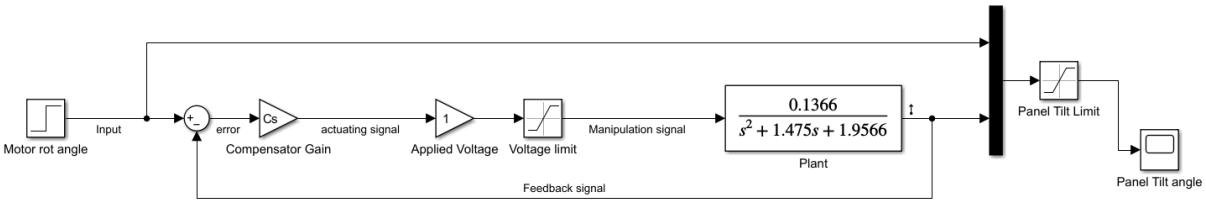


*Figure 27: Root Locus Technique Block Diagram*

Root locus technique assist in the visualization of the effect of PID on the system's behaviour. The system is stable by editing the compensator gain until the system stabilises [25]. To properly understand the system the transfer function of the PID is illustrated below:

$$G(s) = \frac{40.98s + 34.15}{s^3 + 1.475s^2 + 42.94s + 34.15}$$

Which suggests that the system will have three poles and one zero, therefore the root locus will help us visualise the motion of poles in the s-plane, therefore determine the transient response characteristics. The poles of the transfer function above have negative real parts which suggests that the PID system is stable.

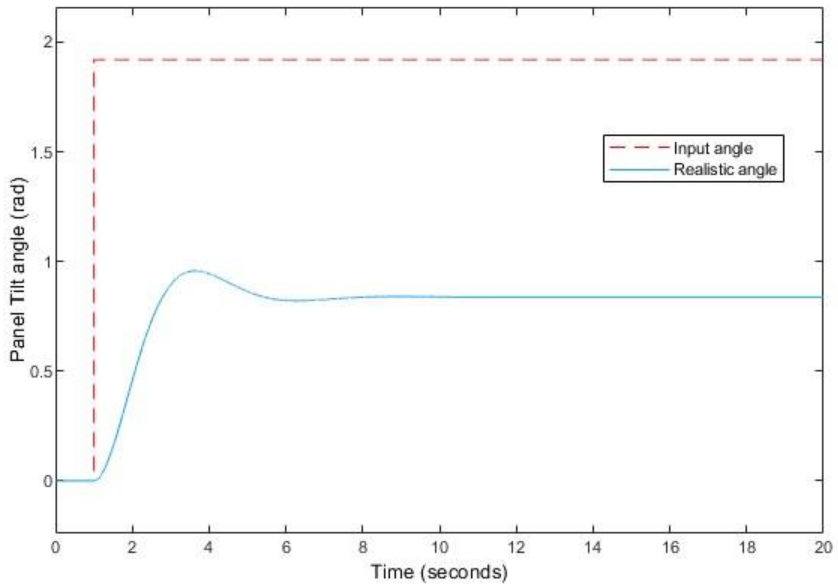


*Figure 28: Root locus Tilt Response*

The root locus response illustrated by figure 1 above was constructed with different compensator gains. Since the pole roots are moved through the root locus, the performance specification requirements have to be satisfied. A constant input angle was directed into the closed loop and the most realistic gain was found to be 70.82.

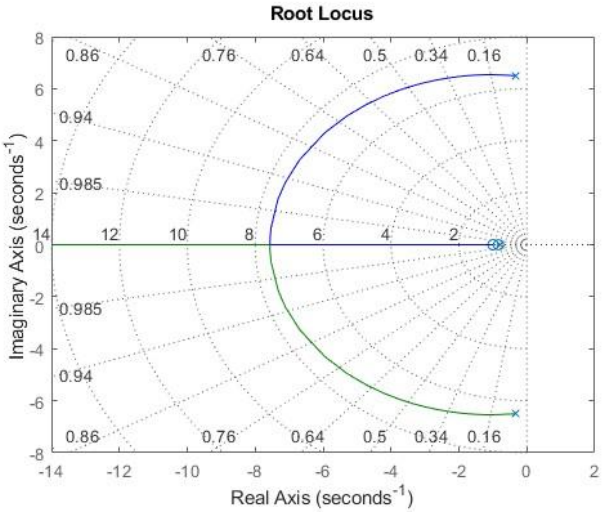


*Figure 29: System Root Locus Technique*

With lower values of K, marginal stability was experienced which suggested that disturbances pushed the system into instability mainly due to Perturbations. The input gain K is changed from zero ranging to infinity, the poles vary along each branch of the root locus. By examining the movements of the poles, the root locus controller was

designed with a gain of 70.82 which suggested the system was stable by shifting the poles in the left-hand side of the real axis. The system will remain stable under specified initial conditions.

*Table 8: Root Locus Specifications*

| | Panel Tilt Angle | |
|---|---|---|
| Specification | Desired outputs | RL outputs |
| Frequency (Hz) | > 0.875 | 4.28 |
| Peak (rad) | ≤ 1.2 | 0.91 |
| Peak time (s) | < 5 | 2.45 |
| Overshoot (%) | < 20 | 8.3 |
| Undershoot (%) | < 20 | 1.16 |
| Steady state error (%) | ≤ 5 | 0.356 |
| Rise Time (s) | ≤ 0.4 | 0.249 |
| Settling time (s) | < 5 | 3.6 |
| Transient Time (s) | - | 3.6 |

Table 10 above suggests that the root locus technique results in values almost similar to the PID. The frequency was found to be 4.28 Hz which was greater than 0.875, higher frequency suggests that the system root locus system at 70.82 responds more quickly, with accuracy. High frequency suggests that the panel can follow the sun's location faster [26]. Both Peak and percentage overshoot obey the desired outcome, which suggests that the voltage limit to the system restricts excessive voltage which will result in high peak values leading to early instabilities experienced. Rise time was found to be 0.249 which meets the desired outcome criteria, as illustrated by figure 1 above, poles are far from the imaginary axis, therefore a higher rise time is suitable, which suggests than the natural frequency of the panel is high. Settling time was found to be 3.6 which satisfy the desired specs, the poles in the root locus are positioned in the left half of the real axis which suggests that the system results in a faster settling time [26].

$$t_s = \frac{4}{\varsigma w_n}$$

To satisfy equation above, the denominator should be 1.11, since the damping coefficient for the uncontrolled system was 0.3, the natural frequency to obtain a realistic settling time should be 3.7037 rad/s. the steady state error is the difference of the desired and actual outputs, the root locus assed was the type zero system which suggests that the error depends on the gain adjustments [27]. A gain of 70.82 reduced the steady state error from high percentages to 0.356 but slightly affects the stability.

# 6. EVALUATION OF THE SIMULATION SYSTEM

In this section, the evaluation and analysis of the controlled system were conducted. A PID controller was employed to stabilize the system plant, enhancing the overall system's robustness in response to various inputs. The PID controller integrates proportional, integral, and derivative controls, each offering distinct functionalities. Although PI or PD control systems could have been used, implementing all three controller gains was essential to minimize and eliminate the steady-state error. Additionally, the Root Locus Technique was utilized to fine-tune the PID controller, potentially modifying the system's transfer function to achieve optimal performance.

### 6.1 Analytical Evaluation Of The Control System

Different Controller method were implemented to analyse system stability, a PID resulted in a stable system nut was further fine-tuned through utilising a root locus controller but was analysed by simulation results only. The transfer function of the PID was evaluated using different compensator gains until stability is reached. The denominator of the analysed transfer function is the system's characteristic equation which can be analysed analytically using the Routh-Hurwitz method which is analysed below:

$$Poles = Char\ eq = s^3 + 1.475s^2 + 42.94s + 34.15$$

From the characteristic equation above, the controller array can be analysed as follows:

*Table 9: Routh-Hurwitz Array*

| | | |
|---|---|---|
| $s^3$ | 1 | 42.94 |
| $s^2$ | 1.475 | 34.15 |
| $s^1$ | 19.8 | 0 |
| $s^0$ | 34.15 | 0 |

Using the Routh-Hurwitz criterion analysis, it can be suggested that the system is stable because there is no sign change observed in the first column. Table 1 above satisfy the Routh-Hurwitz array stability check and furthermore, poles of the characteristic equation can be analysed by finding the nature of the real part and determining the stability as illustrated below.

$$s_1 = -0.8054$$

$$s_2 = -0.3348 + 6.503i$$

$$s_2 = -0.3348 - 6.503i$$

The system has poles with negative real parts which indicates that the system is stable. Furthermore, the system satisfies the analytical BIBO stability analysis which states that if the poles lie in the left half of

the complex plane the system is BIBO stable and will maintain stability under specified operating conditions.

The performance of the solar tracker is affected by the error signal from the feedback to the control unit which affects the system's accuracy and quality to maintain desired outs from specified inputs. The steady state error of the system is reduced through utilizing fine tuning controllers such as PID and root locus. No integrators involved in the tuning controller; a finite steady state error is expected which will be analysed below.

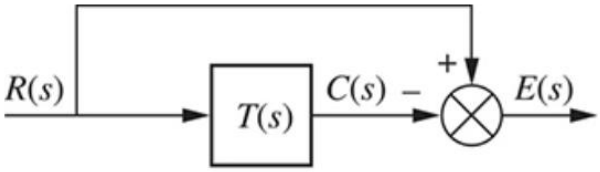


*Figure 30: Closed-loop transfer function [27]*

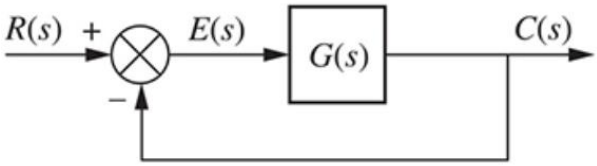


*Figure 31: Open-loop transfer function*

From the figures above it is evident that [27]:

$$E_{(S)} = R_{(S)}[1 - T_{(S)}]$$

$$T_{(S)} = \frac{40.98s + 34.25}{s^3 + 1.475s^2 + 42.94s + 34.15}$$

From chapter 7.2 of the Mechatronics Zybook text, an error signal is analysed as follows [27]:

$$e(\infty) = \lim_{n\to\infty} e(n) = \lim_{s\to 0} sE(s)$$

$$\therefore\ e(\infty) = \lim_{s\to 0} sR_{(S)}[1 - T_{(S)}]$$

$$e(\infty) = \lim_{s\to 0} \frac{0.0349}{s}\left(\frac{s^3 + 1.475s^2 + 83.93s + 68.3}{s^3 + 1.475s^2 + 42.94s + 34.35}\right)$$

$$e(\infty) = 0.01156$$

The error found indicates the deviations between the expected panel location and the actual position of the tracker. The signal suggests a high level of accuracy of the tracker through which the panel angle is aligned with the best angle to obtain maximum intensity of the sun. 0.01156 implies tracking reliability

as it operates near its peak, this suggests that the PID and the root locus are fine-tuned which will produce the required power to sustain the irrigation system throughout the day.

### 6.2 Simulation Evaluation Of The Control System

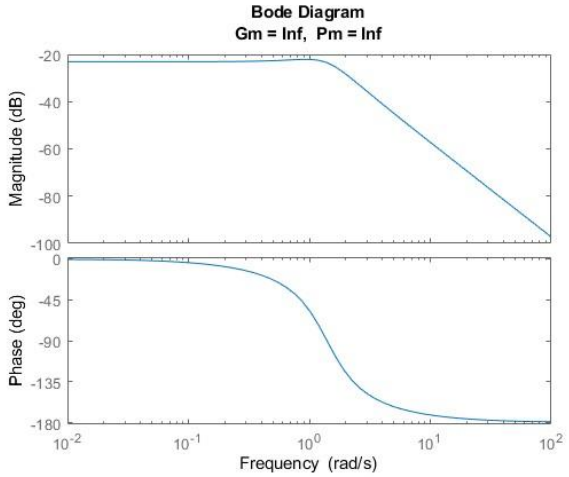


*Figure 32: PID Bode Plots*

The provided Bode plot reveals the dynamic performance of a well-tuned PID controller across various frequency ranges, characterized by a consistent -20 dB gain at low frequencies and a roll-off that begins at -20 dB/decade and steepens at higher frequencies. This behaviour indicates effective integral control at low frequencies, which helps eliminate steady-state errors by responding strongly to sustain input errors. As the frequency increases, the proportional and derivative components of the PID controller become more dominant. The gradual phase decrease from near 0 degrees to -180 degrees across the frequency spectrum illustrates the increasing influence of the proportional control, which introduces a phase lag, stabilizing the response to changing inputs. At higher frequencies, the significant phase lag introduced by the derivative component helps dampen the system's response to rapid changes, enhancing overall stability and reducing overshoot. This interpretation of the Bode plot underscores the PID controller's robust performance, ensuring a balanced response that effectively manages stability, minimizes steady-state errors, and provides dynamic control over a wide range of operating conditions.

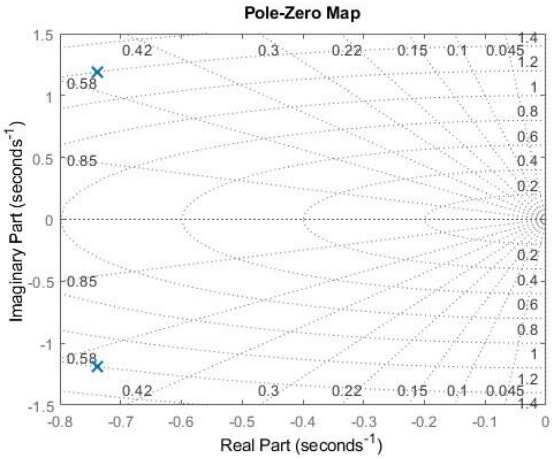


*Figure 33: Pole-Zero Map Of The PID*

The given pole-zero map indicates the system's poles at -0.42 ± 0.58i, showing stability as all poles are in the left side of the complex plane. Complex conjugate poles indicate damped oscillations, where the real part (-0.42) determines the decay rate and the imaginary part (±0.58) sets the oscillation frequency. The lack of zeroes in the observable region simplifies the system's dynamics. The pole and zeros map above shows that the PID controller was properly set to produce a consistent, well-damped response. Proportional control optimizes overall system gain; integral control removes steady-state error; and derivative control improves transient response by eliminating overshoot. The PID controller successfully alters the system's dynamics, resulting in the desired stability and performance

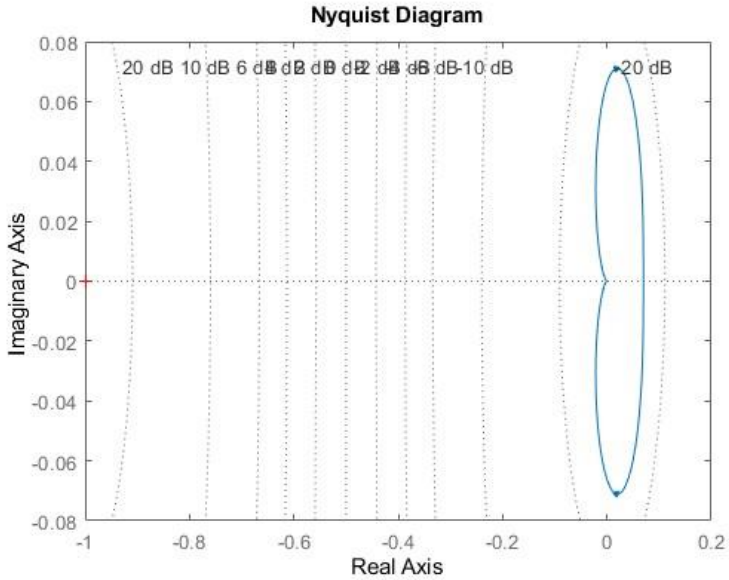


*Figure 34: PID Nyquist Plot*

The Nyquist plot displays the frequency response of a control system with a PID controller, providing information on its stability and performance. The plot above shows that the system does not encircle the

critical point (-1,0), indicating that it remains stable as in section 4.3.5.3 of the report. The plot's elliptical shape indicates that the PID components have a balanced influence: the proportional control adjusts the system's overall gain, the integral control helps eliminate steady-state errors by keeping the plot close to the origin, and the derivative control provides damping by shaping the high-frequency response. The small deviation in the imaginary axis suggests that the derivative action successfully reduces overshoot and improves stability without creating large phase lead, which could lead to instability. The proximity of the plot to the real axis also highlights that the proportional and integral actions are finely tuned, ensuring a stable and responsive system.

### 6.3 Instrumentation To Fully Implement The Solar Controller

For the solar sun tracker to fully function autonomously, a controller is required. Control system includes instruments such as sensors, controllers, and algorithms. The instrumentations required are discussed below:

- **Photoelectric (Light Sensor)**

  Employed to detect sun location due to its ability to detect ambient light. When light is incident to the transistor, current flow is induced which transfers to the control unit. Four light sensors should be positioned on corners o determine the sun intensity which determines the sun's location. Can be used on the solar sun tracker to detect changes in the sun position and perturbations experienced during the tracking process [28].

- **Encoder (Position Sensor)**

  Sun tracker is rotating about the pivot point which requires rotary encoders which measures the rotational position of the panel and are assembled to the panel about the rotational axis. They can be used in the sun tracker for motion control through panel velocity and provides motion feedback and transferred to the control unit [29].

**Motor Encoder**

- **Incremental Encoder**

  Encoder which converts the angular position of a motor shaft into a digital code that can be input into the control unit to identify the angular position. A servo motor that features an incremental encoder can be used in the solar sun tracker to identify the angular position of the motor before and after the gearbox in order to calibrate the panel's angular position with the actual sun position [30].

**Controller:**

- **Programmable Logic Controller**

All sensors included in the system are monitored by the Programmable logic controller. A closed-loop control system is required. PLC monitor the input values against the custom program and make adjustments to suit the required output. It should be fitted on the solar sun tracker to run tracking algorithm and adjusts the panel to align with the location of the sun properly [31].

**Predictive Model:**

- **Solar Ephemeris data**

Digital solar position code which provides an algorithm which determines the location of the sun due to geographical location and season of the year. Can be utilized in the solar tracking system (based on the Karoo data) as an input angle into the PID controller and find the output suitable position from input angle signals which actuates the motor [32].

- **Inertial Measurement Unit (IMU)**

A typical IMU consists of gyroscope, accelerometer and a magnetometer which operate in a single axis. The equation of motion of the solar panel requires angular velocity and position which suggest that an IMU in required to obtain the required system balance by eliminating rotational vibrations. Aerodynamic drag is one of the disturbances which are experienced and causes system vibrations which requires an IMU for detection and resolving through the controller [33].

**Charge Controller:**

- **Maximum Power Point Tracking Charge Controllers (MPPT)**

The solar tracking system is required to power the centre pivot irrigation system, therefore a MPPT controller is required to make sure that maximum power is produced by the solar panel to keep the system operating throughout the day. It is useful due to its ability to extract more power from the tracker under fluctuating sun intensity [34].

# 7. BONUS QUESTION

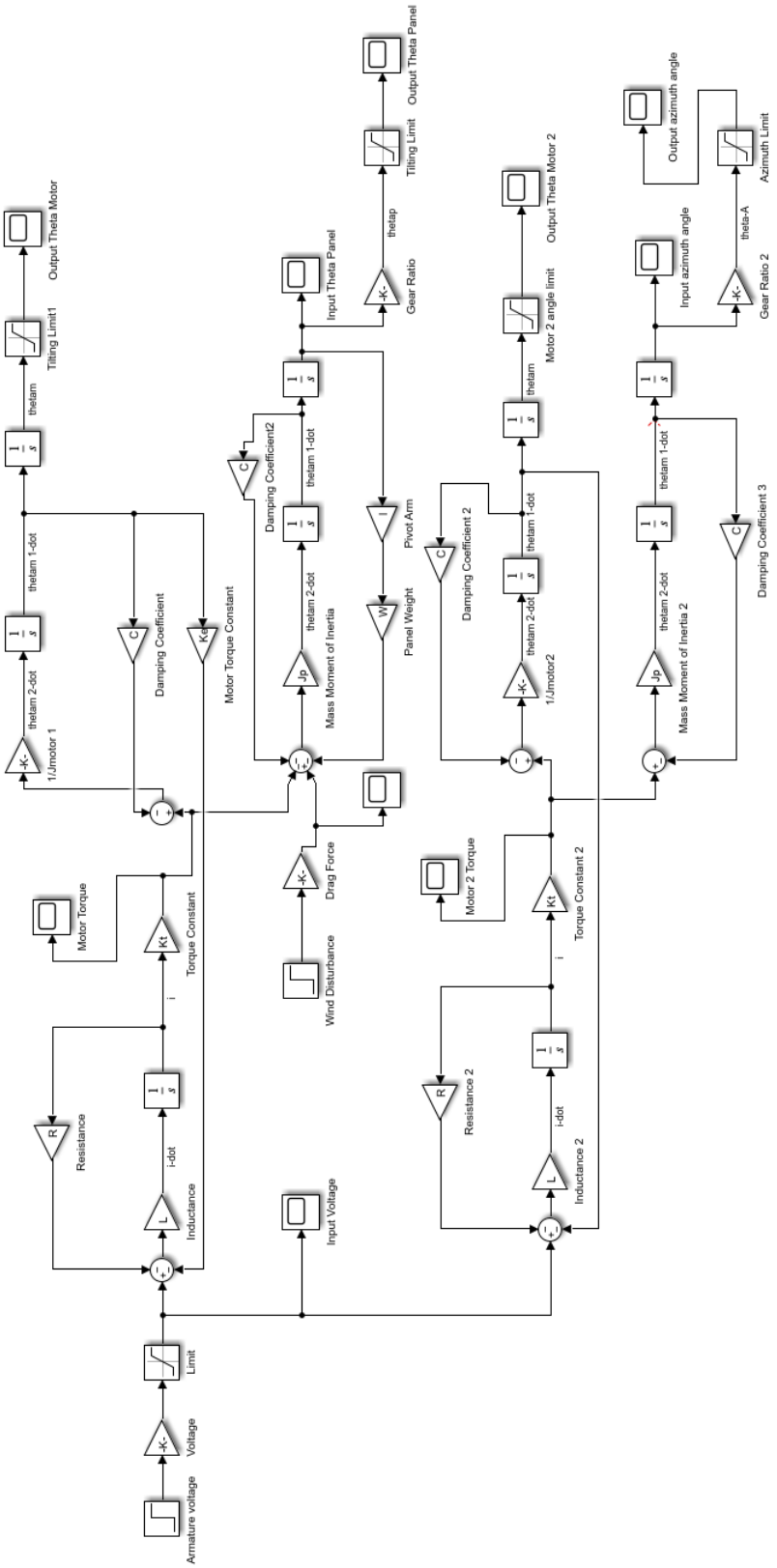


*Figure 35: Zenith And Azimuth Uncontrolled Model*

Motion of the panel around the axes is independent which suggests that they are supplied by the same voltage but rotated independently based on the feedback from the sensors. The dual axis tracker will be designed in such a way that the zenith tracker designed in previous parts will be joined with the azimuth tracker that will be developed in this section to obtain a fully operational dual-axis tracker.

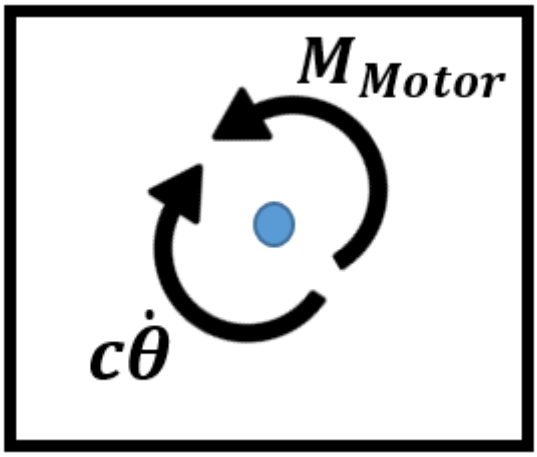


*Figure 36: Azimuth Rotation Freebody Diagram*

$$J\ddot{\theta} = \frac{k_t(V_a - k_e\dot{\theta})}{R} - c\dot{\theta} - wl\sin\theta + F_D l\cos\theta$$

**Panel Equations:**

$$J\ddot{\theta} = T - c\dot{\theta}$$

$$\ddot{\theta} = \frac{1}{J}\left(\frac{Kt}{R}\left(V_A + K_E\dot{\theta}\right) - C\dot{\theta}\right)$$

**Motor Equations:**

$$J_{motor}\ddot{\theta} = \left(\frac{Kt_{motor}}{R}\left(V_A + K_{Emotor}\dot{\theta}\right) - C_{motor}\dot{\theta}\right)$$

Panel's non-linearized mass Moment of Inertia [9]:

$$J = \frac{m}{12}(l^2cos^2\theta + d^2sin^2\theta + c^2)$$

Panel's linearized mass Moment of Inertia:

$$J = 0.8682 + \frac{21}{12}(2d^2\theta - 2l^2\theta)$$

### 7.1 Time responses of the uncontrolled dual axis solar sun tracker

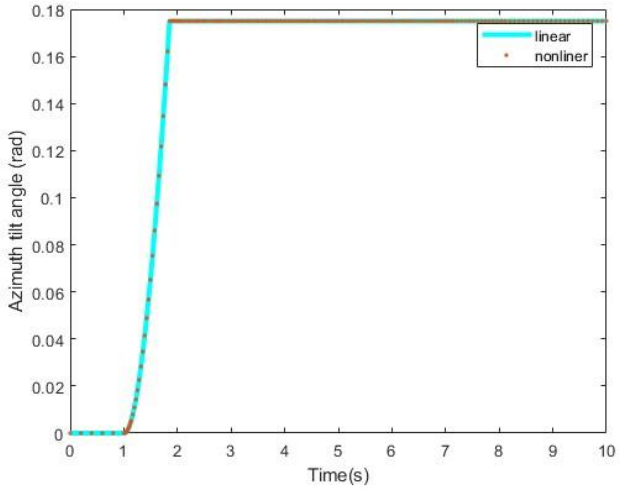


*Figure 38: Azimuth step Input*

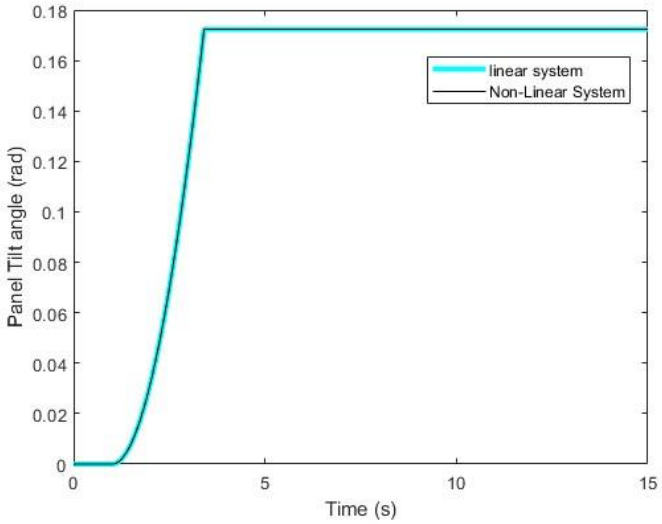


*Figure 37: Zenith Step response*

As illustrated by figure 37 above, the azimuth step response is similar fir both linear and nonlinear system. This suggests that the linearization performed was appropriate in the azimuth angle. The plots suggested that a 1.5% error was observed between the linear and nonlinear systems. A saturation limits the angles at 0.175 which restricts the system to pass through higher angles where larger errors are experienced.

The time response of the zenith angle was analysed in the uncontrolled response section of the tilting solar sun tracker and had an error of 1.568% between a linear and non-linear response. A positive tilting angle suggests that a positive voltage signal was input into the system because results in a clockwise rotation from the east, tracking to the west, rotationally. The uncontrolled system rotates infinitely since feedback systems are not utilized therefore saturation was used to limit excess voltage.

**Frequency Domain Response**

Bode plot

A bode plot is required to critically analyse the azimuth linearized system in a Frequency domain. Bode plots can also be used to evaluate different rotational frequencies and analysing the resulting behaviour. In order to analyse stability, the azimuth system has to be understood through Bode plots by determining the frequency, phase margin, gain margin and bandwidth. The stability criterion will be achieved when higher phase and gain margin are obtained.

The azimuth Bode plot was obtained from the transfer functions below**:**

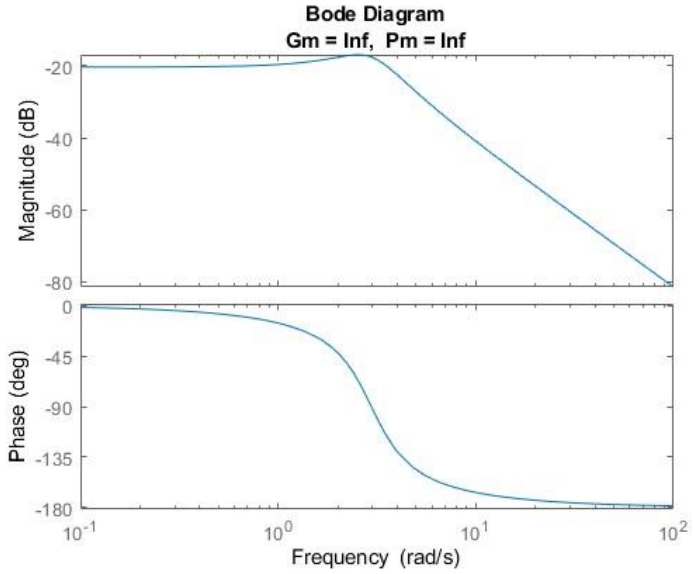


*Figure 39: Bode Plot of the Azimuth tracker*

As illustrated by figure 3 above, both the gain and phase margin are infinite because both the phase and magnitude never reaches a Frequency of 0dB. This analysis suggests the system is stable due to infinitely high margins. The bandwidth was interpreted from the bode plots with a maximum value of approximately 1400 dB which is higher than both the phase and gain margins. The bandwidth value suggests that the system respond very quickly and can result in experiencing instabilities.

A control system is required for the azimuth tracking to ensure that tracker does not fluctuate during tacking which will lead to large tracking deviations. Tasks required from the azimuth tracker are not time invariant therefore Nyquist stability criterion will be used to analyse the time invariant azimuth system due to encircling points to determine stability.

## Nyquist Plot of the Azimuth Tracker

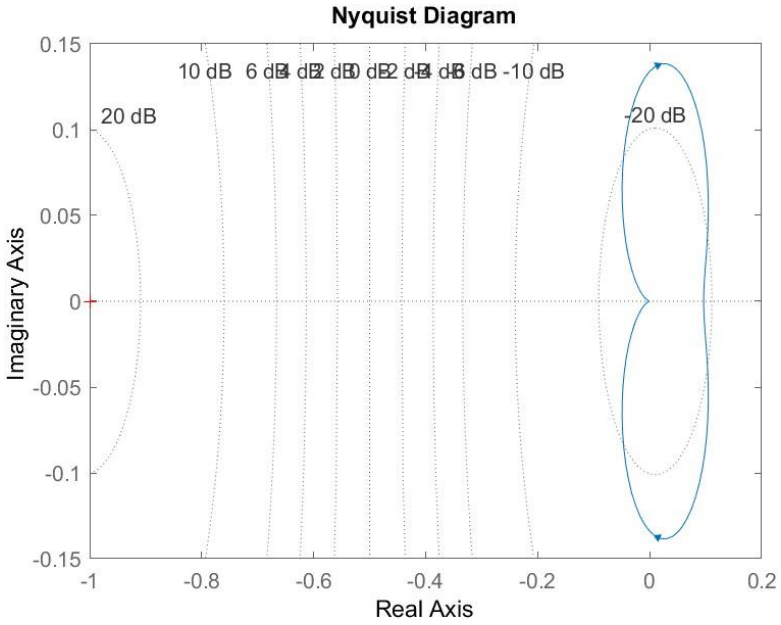


*Figure 40: Nyquist Plot of the Azimuth Tracker*

As illustrates in figure above, the Nyquist plot is clockwise and lies outside the (-1, 0) point which suggests that the system is marginally stable. But the zeros in the system do not satisfy the Nyquist stability criterion, because the Zero obtained is equals to 0 which suggested that the system is unstable. Furthermore, there are two poles just about the 0 axis which suggests that the system is unstable. It can be deduced that the system is unstable.

### Controller Design

As previously analysed in the zenith solar tracker, a controller design was required to obtain required stability. Instabilities were experienced in the azimuth tracker which suggests that a control system is required to ensure the system maintains stability under normal operating conditions. Azimuth angle of rotation will be used to analyse the system stability.

### Proportional integral derivative technique

A closed loop system is required to attain stability of the system by utilizing a feedback controller. Feedback from the sensor is required to adjust controller due to output error and actual Azimuth angle.

The figure below illustrates the azimuth PID controller block diagram for the azimuth tracker:

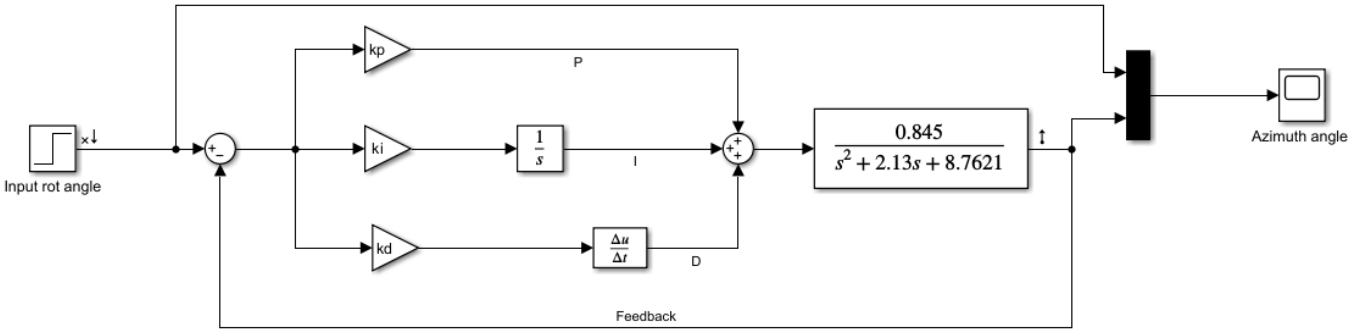


*Figure 41: PID Controller of the Azimuth tracker*

To fine tune the system an angle of 0.2 radians was input to the system to analyse disturbances experienced during rotation. Different gains were input to the system iteratively until stability was obtained. The realistic gains were almost similar to the zenith tracker with Kp = 290, ki = 220, and Kd = 89 which resulted in a response plotted in figure 5 below.

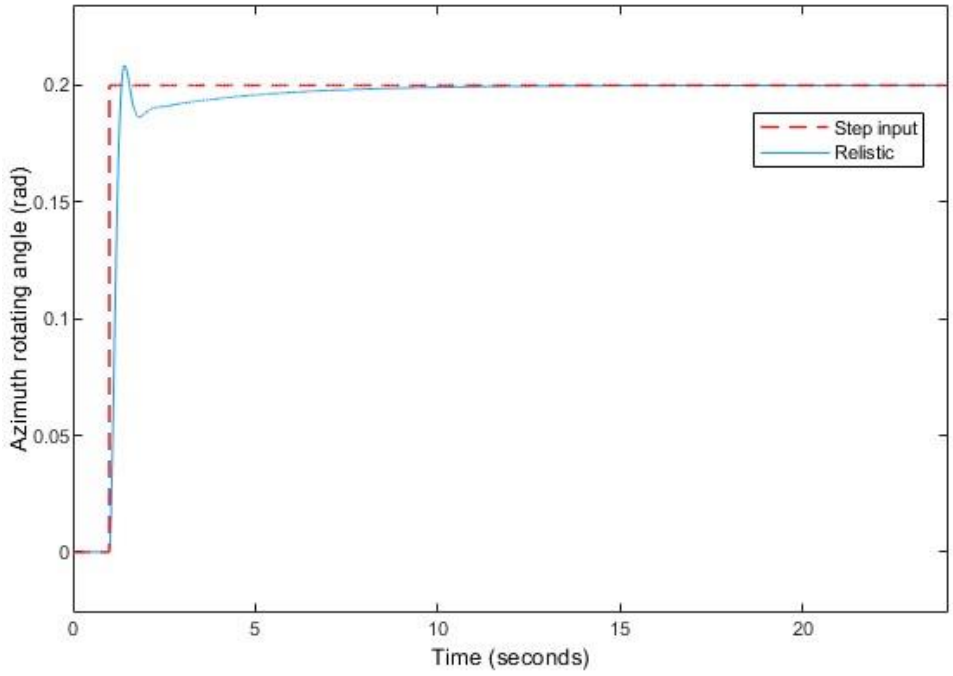


*Figure 42: PID response of an azimuth tracker*

**Root locus**

The Root Locus found has poles immediately just after the 0 which suggests that the system was marginally stable, and due to gains iteratively changing, the system became stable because the all poles lie in the left half of the real axis.

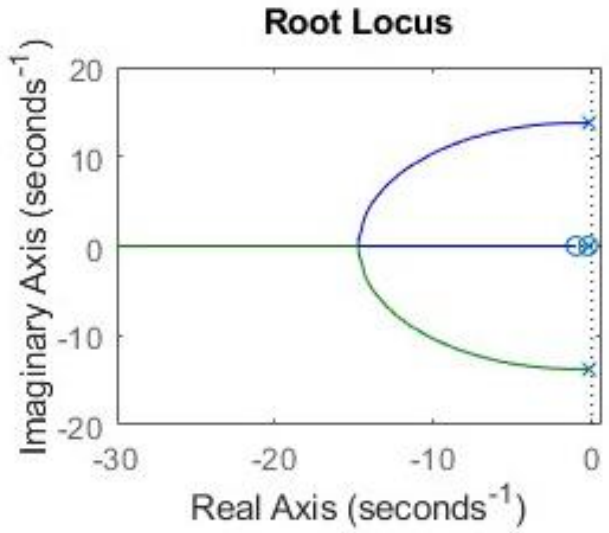


*Figure 43: Root-locus plot of the azimuth tracker*

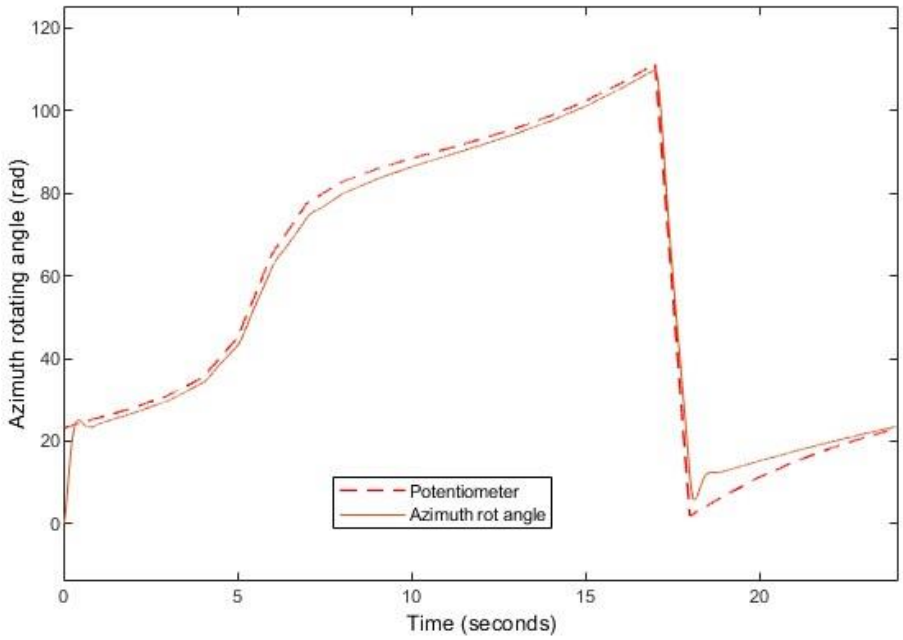


*Figure 44: Azimuth rotating angle with potentiometer*

The azimuth tracker follows the potentiometer throughout the day with small deviations, as illustrated by Figure 6 above. Assuming that the tracker switches on at 00h00, which is the datum. At around 06h30, up until 09h00 a steep increase in angle is experienced which is due to the balancing between the zenith and azimuth to maximize sun Intensity, and there are fluctuations expected to happen in the morning hours. The system stabilizes around

10h00 up to 18h00, where the sun set will be experienced. steep angle drop is experienced around 19h00 to return to its original position 0f zero degrees, then goes back to the initial position throughout the night.

## Discussion

Independent axes were considered in the dual-axes tracker where an individual single axes tracker (Zenith) was developed in the previous chapters. Another single axis tracker was designed in the bonus question (Azimuth) to properly absorb energy from the sun which is more flexible than the Zenit tracker due to experiencing fewer external disturbances such as aerodynamic drag. The dual-axis tracker increases the solar panel efficiency by about 30% as compared to the individual single-axis tracker. Potentiometers installed on the sensor enhances maximum sunlight intensity to the tracker which suggests that even during cloudy weather conditions, the irrigation system will be powered effectively.

## 8. DISCUSSION

The objective of this project was to design a control system for efficient tracking of the sun's path, ensuring that the solar panel maintained the optimal angle for energy absorption throughout the day for farming purposes in Bredasdorp. To ensure precise direct sunlight tracking, online databases were utilized to collect solar position data specific to Bredasdorp. This data illustrated the sun's position in the sky throughout the year. Additionally, a nonlinear model was developed to accurately represent the tracker system's dynamic behaviour. This model was essential for evaluating the uncontrolled system's performance in both the time domain (transient response) and the frequency domain (stability characteristics).

The uncontrolled results for the system were retrieved through detailed time-domain and frequency-domain analyses. Initially modelled as an uncontrolled plant in Simulink, the system's performance was evaluated using transient response functions namely, step, ramp, impulse, and sinusoidal inputs. Disturbances, including voltage and aerodynamic drag, were limited to specific ranges based on motor specifications and panel design constraints. These disturbances were applied, and the system's responses, particularly in terms of tilting angle and stability, were analysed. Additionally, frequency-domain analysis using Bode plots illustrated the system's magnitude and phase response to various input frequencies. This comprehensive analysis showed that the uncontrolled system exhibited partial stability, highlighting the necessity for a controller to achieve precise sun tracking.

The PID controller implemented in the solar tracking system demonstrates robust performance in achieving the desired specifications. The Nyquist plot analysis in figure 33 confirms the system's stability, as it does not encircle the critical point (-1,0). This stability is further evidenced by a phase margin of 61.6 degrees and a delay margin of 0.749 seconds at a frequency of 1.44 radians per second, indicating robustness against instability and time delays. The controller effectively minimizes steady-state error, achieving an actual steady-state error of 2.01%, well within the desired threshold of less than 5%. Dynamic performance metrics are also impressive, with a rise time of 0.264 seconds and a settling time of 1.42 seconds, both comfortably meeting the specified requirements of less than 0.4 seconds for rise time and less than 5 seconds for settling time. Additionally, the controller maintains a percentage overshoot of 16.9%, below the desired threshold of 20%, ensuring good transient performance without excessive oscillations or instability. These results illustrate that the PID controller provides a balanced response, effectively managing stability, minimizing steady-state errors, and ensuring dynamic control over a wide range of operating conditions

To fully implement the controller for the solar tracking system, several key pieces of instrumentation are required. Photoelectric sensors are essential for detecting the position of the sun. Four light sensors are placed at the corners to determine the sun's intensity and location, which is crucial for the accurate positioning of the solar panels. Encoders (position sensors) measure the rotational position of the solar panels, providing feedback necessary for precise control and adjustment based on the sun's movement. Incremental encoders (motor encoders) convert the angular position of the motor shaft into a digital code, allowing for precise calibration of the panel's angular position relative to the sun, which is critical for both initial setup and ongoing adjustments during operation. A Programmable Logic Controller (PLC) monitors all sensor inputs and adjusts the panel position based on a pre-programmed algorithm, ensuring that the solar tracker operates

autonomously and accurately adjusts to changes in the sun's position. Solar ephemeris data provides the algorithm for determining the sun's location based on geographical location and season, serving as an input for the PID controller to adjust the panel's position accurately. An Inertial Measurement Unit (IMU), which includes a gyroscope, accelerometer, and magnetometer, is used to eliminate rotational vibrations and disturbances like aerodynamic drag, ensuring the system remains stable and balanced.

If one of the states is not measurable via standard instrumentation, additional steps may be necessary. State estimation techniques, such as the Kalman filter, can be used to estimate unmeasurable states based on measurable outputs and a model of the system dynamics. This allows for the continuous estimation and adjustment of the system state even in the absence of direct measurements. Installing additional sensors that can indirectly measure or infer the unmeasurable state might also be necessary, such as using a combination of position and velocity sensors to estimate acceleration. Model-based control, utilizing a detailed mathematical model of the system to predict the unmeasurable states, can also be employed. This model can be continuously updated with measurable data to improve its accuracy and reliability in estimating the unmeasurable states. By incorporating these additional methods, the control system can maintain accurate and reliable performance even when some states cannot be directly measured.

## 9. CONCLUSION

The project aimed to design a dual-axis solar tracker to optimize solar energy absorption for farming purposes in Bredasdorp. This system independently controls azimuth and zenith rotations, using feedback from sensors to adjust the solar panel's position. The azimuth tracker, developed alongside a previously designed zenith tracker, enhances flexibility and reduces disturbances such as aerodynamic drag, contributing to a 30% increase in efficiency over single-axis systems. Analysis revealed a minor error in both azimuth and zenith tracking, indicating effective linearization and highlighting the need for a control system to address instability. The frequency domain analysis showed high bandwidth and stability margins, while the Nyquist plot suggested marginal stability due to poles near the zero axis.

To stabilize the system, a PID controller was implemented, providing robust performance with a low steady-state error and satisfactory dynamic metrics. The controller's efficiency is demonstrated through the system's quick response times and minimal overshoot, ensuring reliable sun tracking throughout the day. Essential components for implementation include photoelectric sensors for sun detection, encoders for precise panel positioning, a PLC for autonomous operation, solar ephemeris data for sun location, and an IMU to counteract rotational disturbances.

In conclusion, the dual-axis solar tracker significantly enhances solar energy absorption by maintaining optimal panel orientation. The integration of azimuth and zenith rotations allows the system to efficiently follow the sun's path, crucial for maximizing energy yield. The project's success lies in the effective design and implementation of the PID controller, ensuring stability and precision in tracking, ultimately benefiting agricultural operations in Bredasdorp by providing consistent and efficient solar power.

# REFERENCES


[1] 75 (2017) *South Africa - Energy, International Trade Administration | Trade.gov*. Available at: https://www.trade.gov/country-commercial-guides/south-africa-energy (Accessed: 03 March 2024).

[2] *Let's move mountains to address the energy challenge in the Agriculture Sector* (no date) *Western Cape Government*. Available at: https://www.westerncape.gov.za/news/lets-move-mountains-address-energy-challenge-agriculture-sector (Accessed: 03 March 2024).

[3] *Bredasdorp, South Africa - Sunrise, Sunset, dawn and dusk times for the whole year* (no date) *Gaisma*. Available at: https://www.gaisma.com/en/location/bredasdorp.html (Accessed: 03 March 2024).

[4] Sela, G. (2023) *Center Pivot Irrigation Systems*, *Cropaia*. Available at: https://cropaia.com/blog/center-pivot-irrigation/ (Accessed: 03 March 2024).

[5] Awasthi, A., Shukla, A.K., SR, M.M., Dondariya, C., Shukla, K.N., Porwal, D. and Richhariya, G., 2020. Review on sun tracking technology in solar PV system. *Energy Reports*, *6*, pp.392-405.

[6] (No date) *Tracker data sheet - pia solar*. Available at: https://piasolar.com/assets/downloads/Tracker_documentation.pdf (Accessed: 06 March 2024).

[7] (2019) *What's the point of a dual-axis tracker?*, *Smartflower*. Available at: https://smartflower.com/blog/whats-the-point-of-a-dual-axis-tracker/ (Accessed: 17 March 2024).

[8]Available:file:///C:/Users/2320283/Downloads/MECHATRONICS%20II%20Assignment%202024%20Project%20B%20Solar%20Tracker%20(2).pdf. [Accessed 18 March 2024].

[9] Wikipedia, "Season," Encyclopedia, 2023. [Online]. Available: https://en.wikipedia.org/wiki/Season#/media/File:Seasons1.svg. [Accessed 18 March 2024].

[10]Stellenbosch,September2017.[Online].Available:https://www.researchgate.net/figure/Depiction-of-the-apparent-path-of-the-sun-as-the-day-and-year-passes_fig5_321353683. [Accessed 18 March 2024].

[11] N. A. a. S. Administration, "The Balance of Power in the Earth-Sun System," NASA, 2022. [Online]. Available: https://www.nasa.gov/wp-content/uploads/2015/03/135642main_balance_trifold21.pdf. [Accessed 18 March 2024].

[12] Electronics Tutorial, "DC Motors," 2023. [Online]. Available: https://www.electronics-tutorials.ws/io/io_7.html. [Accessed 17 March 2024].

[13] S. Dietrich, "Servo Motor vs Stepper Motor: Understanding the Differences," Control Automation, 13 December 2022. [Online]. Available: https://control.com/technical-articles/servo-motor-vs-stepper-motor-understanding-the-differences/. [Accessed 17 March 2023].

[14] Katherine Harper Hall Boone, 2023. [Online]. Available: https://ases.org/wp-content/uploads/2021/11/Determining-the-Accuracy-of-Solar-Trackers-.pdf. [Accessed 17 March 2024].

[15] A. ohamad, "Efficiency improvements of photo-voltaic panels using a Sun-tracking system," Science Direct, 3 November 2004. [Online]. Available: https://www.sciencedirect.com/science/article/pii/S0306261903002319#:~:text=Tilting%20it%20from%20being%20perpendicular,it%20is%20to%20be%20used.. [Accessed 18 March 2024].

[16] Musa, A. et al. (2023a) 'A review of time-based Solar Photovoltaic Tracking Systems', Information, 14(4), p. 211. doi:10.3390/info14040211.

[17] Weather-And-Climate.com (2019) *Bredasdorp climate by month: A year-round guide*, *World Weather & Climate Information*. Available at: https://weather-and-climate.com/average-monthly-Rainfall-Temperature-Sunshine,bredasdorp-western-cape-za,South-Africa (Accessed: 20 March 2024).

[18] *Climate-data.org* (no date) *Bredasdorp climate: Weather Bredasdorp & temperature by month*. Available at: https://en.climate-data.org/africa/south-africa/western-cape/bredasdorp-10532/ (Accessed: 20 March 2024).

[19] Panday, A. (2024) *School of mechanical, Industrial and Aeronautical Engineering*. Johannesburg, Gauteng: Wits University.

[20] D. Hernandes and e. al, "Mechatronic design and implementation of a two axes sun tracking photovoltaic system driven by a robotic sensor," Science Direct, Novemebr 2017. [Online]. Available: https://www.sciencedirect.com/science/article/pii/S0957415817301381. [Accessed 10 May 2024].

[21] R. Baranuik and e. al, "3.6: BIBO Stability of Continuous Time Systems," Libre Texrs Engineering, 2024. [Online]. Available: https://eng.libretexts.org/Bookshelves/Electrical_Engineering/Signal_Processing_and_Modeling/Signals_and_Systems_(Baraniuk_et_al.)/03%3A_Time_Domain_Analysis_of_Continuous_Time_Systems/3.06%3A_BIBO_Stability_of_Continuous_Time_Systems. [Accessed 10 May 2024].

[22] S. S. Kumar, "Design of PID Controller using Root Locus method," Dept. of Aeronautical Engineering, KCT, Coimbatore, 2020. [Online]. Available: https://kctaero.wordpress.com/wp-content/uploads/2016/07/design-of-pid-controller.pdf. [Accessed 10 May 2024].

[23] Emerson, "The PID Controller & Theory Explained," Emerson, 30 March 2023. [Online]. Available: https://www.ni.com/en/shop/labview/pid-theory-explained.html. [Accessed 10 May 2024].

[24] A. A. Abood, "A comprehensive solar angles simulation and calculation using matlab," *INTERNATIONAL JOURNAL OF ENERGY AND ENVIRONMENT*, vol. 6, no. 4, pp. 367-376, 2015.

[25] Math Works, "Root Locus Design," Math Works, 2024. [Online]. Available: https://www.mathworks.com/help/control/ug/root-locus-design.html. [Accessed 16 May 2024].

[26] J. K. Roberge, "4.3: ROOT-LOCUS TECHNIQUES," Massachusetts Institute of Technology, 2022. [Online]. Available: https://eng.libretexts.org/Bookshelves/Electrical_Engineering/Electronics/Operational_Amplifiers%3A_Theory_and_Practice_(Roberge)/04%3A_Stability/4.03%3A_ROOT-LOCUS_TECHNIQUES. [Accessed 16 May 2024].

[27] zyBooks, "7.2 Steady-state error for unity-feedback systems," zyBooks, 2024. [Online]. Available: https://learn.zybooks.com/zybook/ACMECN4029APandayWinter2024/chapter/7/section/2. [Accessed 18 May 2024].

[28] AdaFruit, "Description," AdaFruit, 2024. [Online]. Available: https://www.adafruit.com/product/2831. [Accessed 2024 May 18].

[29] DYNAPAR, "Motor Encoders - Everything You Need to Know," DYNAPAR, 2023. [Online]. Available: https://www.dynapar.com/technology/encoder_basics/motor_encoders/. [Accessed 18 May 2024].

[30] DYNAPAR, "What is an Incremental Encoder?," DYNAPAR, 2023. [Online]. Available: https://www.dynapar.com/technology/encoder_basics/incremental_encoder/#:~:text=An%20incremental%20encoder%20is%20a,most%20commonly%20used%20rotary%20encoders.. [Accessed 18 May 2024].

[31] Inductive Automation, "PLC: Programmable Logic Controller," Inductive Automation, 24 February 2020. [Online]. Available: https://inductiveautomation.com/resources/article/what-is-a-PLC. [Accessed 18 May 2024].

[32] Astro Pixels, "Planetary Ephemeris Data," Astro Pixels, 2021. [Online]. Available: https://astropixels.com/ephemeris/ephemeris.html. [Accessed 18 May 2024].

[33] Vectornav, "WHAT IS AN INERTIAL MEASUREMENT UNIT?," Vectornav, 2023. [Online]. Available: https://www.vectornav.com/resources/inertial-navigation-articles/what-is-an-inertial-measurement-unit-imu#:~:text=An%20Inertial%20Measurement%20Unit%20(IMU)%20is%20a%20device%20that%20can,a%20measure%20specific%20force%2Facceleration. [Accessed 18 May 2024].

[34] NAZ SOLAR ELECTRI, "What is Maximum Power Point Tracking (MPPT)," NAZ SOLAR ELECTRIC, 2023. [Online]. Available: https://www.solar-electric.com/learning-center/mppt-solar-charge-controllers.html/. [Accessed 18 May 2024].

[35] jovanovic, vukica (no date) *Solar tracking angles | download scientific diagram*. Available at: https://www.researchgate.net/figure/Solar-tracking-angles_fig1_306064621 (Accessed: 19 May 2024).

[36] BrownDogGadgets and Instructables (2017) *Simple dual axis solar tracker*, *Instructables*. Available at: https://www.instructables.com/Simple-Dual-Axis-Solar-Tracker/ (Accessed: 19 May 2024).

[37] (2018) *Analysis of Photovoltaic System Energy Performance* ... Available at: https://www.nrel.gov/docs/fy14osti/60628.pdf (Accessed: 19 May 2024).

# APPENDICES

## Appendix A: Engineering Drawings

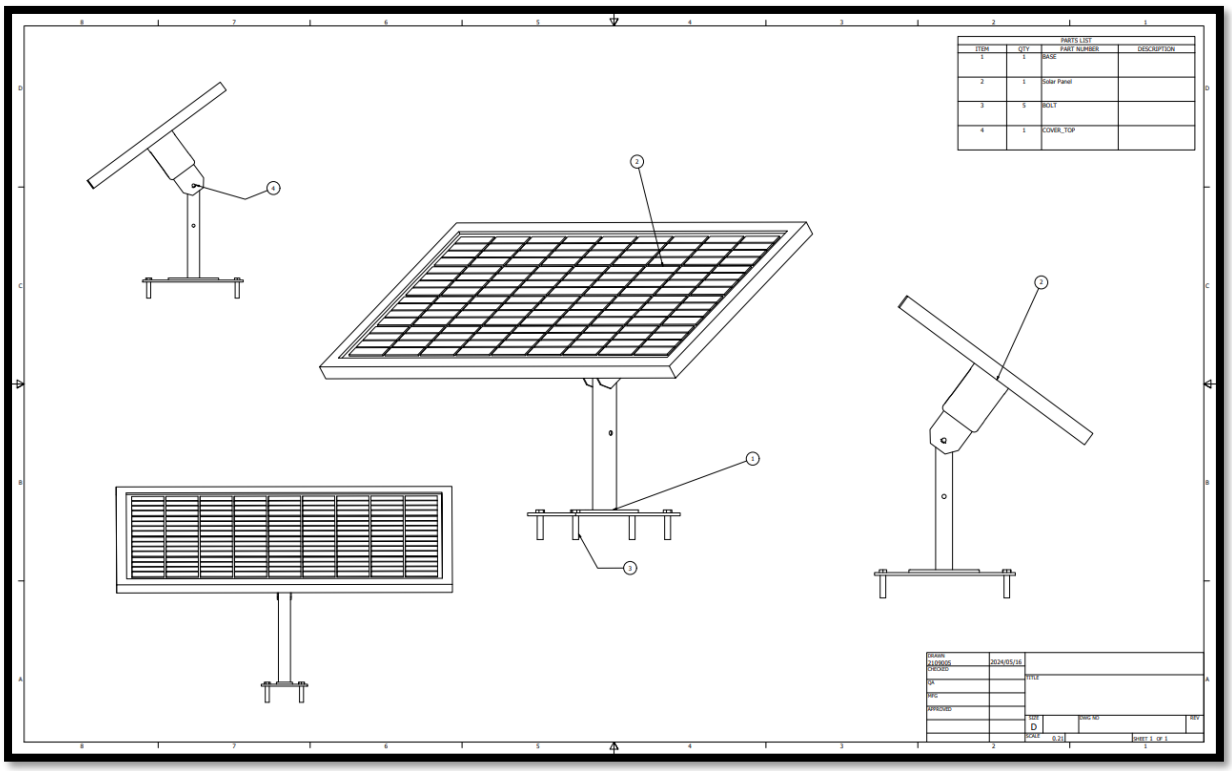

**Appendix B: CAD Drawings**